AGU PUBLICATIONS

Tectonics

RESEARCH ARTICLE
10.1002/2015TC004103

Key Points:
- NW Australia is not a stable continental region
- Faults have been reactivated in Quaternary time
- Active faulting is attributed to crustal transitions on the northern plate boundary

Correspondence to:
J. V. Hengesh,
james.hengesh@uwa.edu.au

Citation:
Hengesh, J. V., and B. B. Whitney (2016), Transcurrent reactivation of Australia's western passive margin: An example of intraplate deformation from the central Indo-Australian plate, *Tectonics*, *35*, doi:10.1002/2015TC004103.

Received 8 DEC 2015
Accepted 24 MAR 2016
Accepted article online 30 MAR 2016
Corrected 23 MAY 2016

This article was corrected on 30 MAY 2016. See the end of the full text for details.

Transcurrent reactivation of Australia's western passive margin: An example of intraplate deformation from the central Indo-Australian plate

J. V. Hengesh[1,2] and B. B. Whitney[3]

[1]Centre for Offshore Foundation Systems, University of Western Australia, Crawley, Western Australia, Australia, [2]Now at Interface Geohazard Consulting, Lahaina, Hawaii, USA, [3]Centre for Energy Geoscience, University of Western Australia, Crawley, Western Australia, Australia

Abstract Australia's northwestern passive margin intersects the eastern termination of the Java trench segment of the Sunda arc subduction zone and the western termination of Timor trough along the Banda arc tectonic collision zone. Differential relative motion between the Sunda arc subduction zone and the Banda arc collision zone has reactivated the former rifted margin of northwestern Australia evidenced by Pliocene to Quaternary age deformation along a 1400 km long offshore fault system. The fault system has higher rates of seismicity than the adjacent nonextended crustal terranes, has produced the largest historical earthquake in Australia (1941 M_L 7.3 Meeberrie event), and is dominated by focal mechanism solutions consistent with dextral motion along northeast trending fault planes. The faults crosscut late Miocene unconformities that are eroded across middle Miocene inversion structures suggesting multiple phases of Neogene and younger fault reactivation. Onset of deformation is consistent with the timing of the collision of the Scott Plateau part of the passive continental margin with the former Banda trench between 3.0 Ma and present. The range of estimated maximum horizontal slip rates across the zone is ~1.4 to 2.6 mm yr^{-1}, at the threshold of geodetically detectable motion, yet significant with respect to an intraplate tectonic setting. The folding and faulting along this part of the continental margin provides an example of intraplate deformation resulting from kinematic transitions along a distant plate boundary and demonstrates the presence of a youthful evolving intraplate fault system within the Indo-Australian plate.

1. Introduction

Major lithospheric transitions along plate boundary systems cause significant changes in structural geometry and style of deformation, such as the initiation or termination of subduction zones, changes from subduction to collisional or transcurrent tectonic regimes, and the triggering of deformation in adjacent intraplate regions. Examples where the transition from one type of crust to another affect the nature of tectonic processes along the Indo-Australian plate include the following: the southern termination of the Hikurangi trench and initiation of the Alpine fault system at the intersection with Chatham Rise in New Zealand [*Wallace et al*., 2004], the eastern termination of the Makran subduction zone and initiation of the Chaman fault zone at the western margin of Indian continental crust [*Jacob and Quittmeyer*, 1979], and the western termination of the Sunda arc subduction zone and transition to the Himalayan collision at the eastern margin of Indian continental crust [*Deplus et al*., 1998]. The eastern termination of the Java trench segment of the Sunda Arc subduction zone at the Indian Ocean crust-Australian continental crust transition (Figure 1) is an additional example of the changes in plate boundary architecture that can occur at these major lithospheric transitions. These changes in plate dynamics cause not only intense local deformation, such as development of transcurrent fault systems, large-scale nappe structures, and thrust fronts (e.g., outer Banda Arc) [*Harris et al*., 2009; *Audley-Charles*, 2011], but also far-field intraplate deformation [*Delescluse and Chamot-Rooke*, 2007]. Seismicity related to the far-field intraplate deformation in the Indian Ocean includes large-magnitude earthquakes such as the 2012 M_w 8.7 Indian Ocean [*Yue et al*., 2012] and the 1906 M_s 7.8 Exmouth events [*Geller and Kanamori*, 1977].

In this paper, we examine the pattern of intraplate deformation occurring along the western continental margin of Australia in response to the changes in structural style and relative motion between the Java trench segment of the Sunda arc subduction zone and the Banda arc collision zone. First, we examine the kinematic framework along the northern plate boundary zone, and then we use exploration seismic data to document a

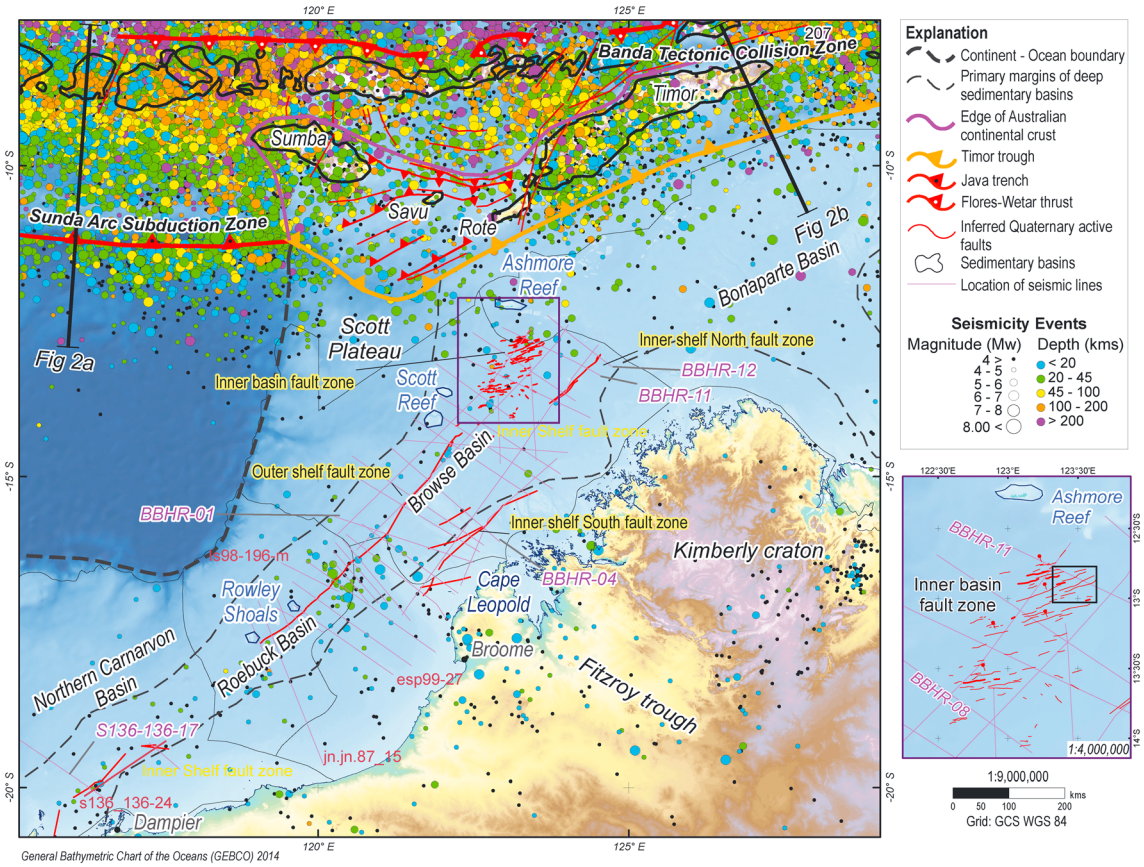

Figure 1. Regional location map showing major tectonic elements and seismicity in the central Indo-Australian Plate. Seismicity catalog compiled from multiple reporting agencies (Table 1). Events of $M_w \geq 0.0$ are shown for period 1815 to 2015. See Figure 2 for a plot of well-located events from the ISC-GEM catalog [*Storchak et al.*, 2013]. Basin boundaries are from Geoscience Australia [*Stewart et al.*, 2013].

system of faults that extends across the Browse, Roebuck, and northern Carnarvon basins on Australia's North West Shelf (Figure 1). In conclusion, we present a tectonic framework for intraplate deformation in the central Indo-Australian plate.

2. Regional Tectonic Setting

The Indo-Australian plate is migrating northward along an azimuth of 011° to 015° at a rate of 75 mm/yr relative to Eurasia (Figure 2) [*DeMets et al.*, 1994] and 66 to 72 mm yr^{-1} relative to a fixed Sunda Shelf reference

Table 1. Reporting Agencies Used to Compile Seismicity Catalog for Figure 1[a]

	Agencies
AUS	Geoscience Australia, Canberra, Australia
AWI	Alfred-Wegener Institute of Seismology
BJI	Beijing, China
BKK	Bangkok, Thailand
DJA	Djakarta, Java, Indonesia. Includes only events north of 13° south latitude.
GCM	Menlo Park, California
GFZ	GeoForschungsZentrum (GFZ), Potsdam, Germany
GS	United States Geological Survey, Denver, Colorado
GS0	United States Geological Survey, Denver, Colorado
ISC	International Seismological Centre, Newbury, UK
ISC-GEM	International Seismological Centre-Global Earthquake Model
KLM	Kuala Lumpur, Malaysia

[a]The catalog is for the period 1815 to 2015 and includes all events greater than M_w 0.0.

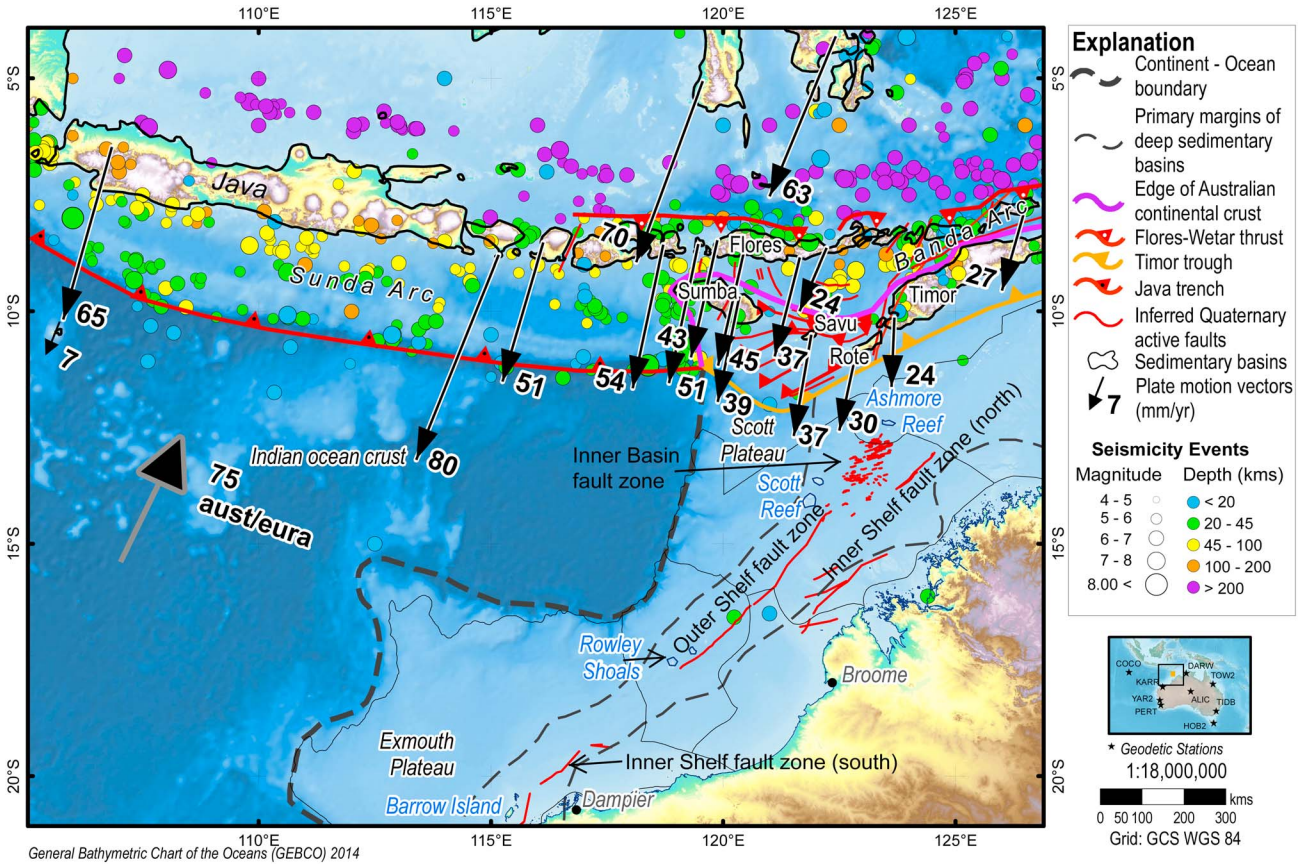

Figure 2. GPS velocities of Sunda and Banda arc region. Large black and grey arrow shows motion of Australia relative to Eurasia [*DeMets et al.*, 1994]. Thin black arrows show GPS velocities of Sunda and Banda arc regions relative to Australia [*Nugroho et al.*, 2009]. Seismicity from ISC-GEM catalog [*Storchak et al.*, 2013]. Note reduction of station velocities from west to east indicating progressive coupling of the Banda arc to the Australian plate compared to the area along the Sunda arc.

frame [*Genrich et al.*, 1996; *Chamot-Rooke and Pichon*, 1999; *Tregoning*, 2003; *Bock et al.*, 2003; *Nugroho et al.*, 2009]. The plate is converging with the Sunda arc subduction zone and the Banda arc tectonic collision zone, which in this region form the northern plate boundary (Figure 1). The northwestern margin of the Australian continent is referred to as the North West Shelf. This region is a passive tectonic margin [*Bird*, 2003] that underwent continental rifting in the Paleozoic and Mesozoic eras [*Yeates et al.*, 1987; *Australian Geological Survey Organization North West Shelf Study Group*, 1994]. The intersection of the Australian continental lithosphere with the northern plate boundary has profoundly changed the style of deformation both along the trend of the plate boundary zone and across the deformation front [*Silver et al.*, 1983; *McCaffrey*, 1988; *Audley-Charles*, 2004, 2011; *Fleury et al.*, 2009; *Harris et al.*, 2009]. There is northward directed Benioff-style (Type B) subduction [*Bally*, 1983] of Indian oceanic crust west of Scott Plateau at ~120°E longitude [*Hamilton*, 1979; *Shulgin et al.*, 2009] (Figure 3a). However, east of this longitude the oceanic crust has been fully consumed and subduction along the middle Miocene age paleo-Banda trench has ceased (Figure 3b) [*Silver et al.*, 1983; *McCaffrey*, 1988; *Hall*, 2011; *Harris*, 1991, 2006; *Audley-Charles*, 2011]. The former subduction zone has become blocked by Australian continental lithosphere and has evolved into an Ampferer (Type A) tectonic collision zone [*Bally*, 1983] where the former accretionary prism has emerged along large-scale nappe structures to form Timor and Sumba islands [*Audley-Charles*, 1975, 1985; *Keep et al.*, 2003; *Duffy et al.*, 2013] and the Suva-Rota ridge [*Roosmawati and Harris*, 2009; *Rigg and Hall*, 2011]. Shortening of ~24 mm yr^{-1} now occurs between Timor and the Australian plate [*Genrich et al.*, 1996; *Bock et al.*, 2003; *Nugroho et al.*, 2009] (Figure 2). As the paleo-Banda subduction zone became blocked and Timor and Sumba islands emerged, the northern margin of the Australian plate began to override the Banda Sea oceanic crust along the Flores-Wetar thrust [*Silver et al.*, 1983; *McCaffrey*, 1988; *Breen et al.*, 1989; *Snyder et al.*, 1996].

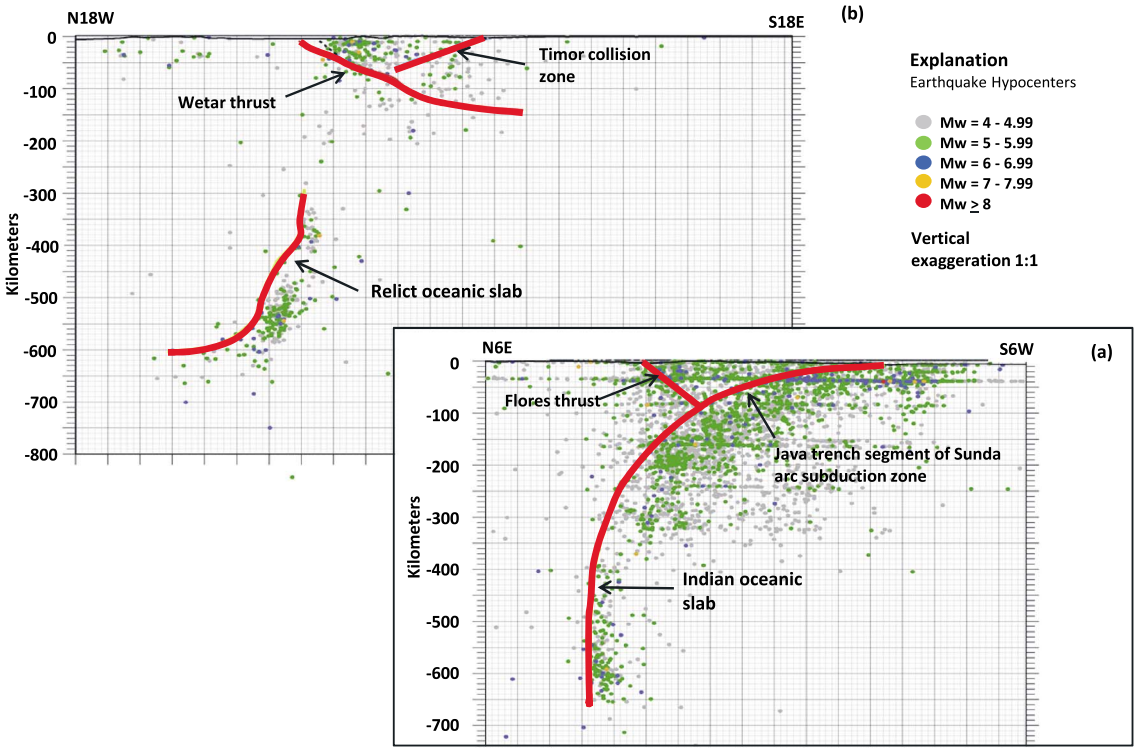

Figure 3. Comparison of hypocentral profiles across the (a) Java subduction zone and (b) Timor collision zone (paleo-Banda trench). Catalog compiled from multiple reporting agencies listed in Table 1. Events of $M_w > 4.0$ are shown for period 1815 to 2015.

Focal mechanism solutions in the region indicate that styles of deformation vary along the length of the northern plate boundary zone, with depth across the boundary zone, as well as along the passive margin of western Australian (Figure 4a). We have plotted centroid moment tensor (CMT) solutions [*Dziewonski et al.*, 1981] from the CMT Project [*Ekström et al.*, 2012] and data from *Revets et al.* [2009] by depth intervals to illustrate variations in patterns of deformation. The area along the outer Banda Arc east of 123°E longitude between Timor and the Timor trough is characterized by shallow (0–19.99 km) to intermediate depth (20–39.99 km) reverse and sinistral reverse-oblique deformation (Figure 4b). This is consistent with the oblique shortening measured between Timor and Australia [*Genrich et al.*, 1996; *Nugroho et al.*, 2009]. Midcrustal to deep-crustal seismicity (>20 km) occurs along the outer continental margin of the Australian plate, south of Timor trough (Figure 1), and available events yield normal focal mechanism solutions (Figure 4b). Geophysical data from the outer Australian continental shelf also show that the dominant style of crustal deformation involves normal faulting related to downward flexure of the continental lithosphere as it becomes involved with the Banda collision [*Langhi et al.*, 2011; *Saqab and Bourget*, 2015]. Deep focus events occur north of the inner Banda arc (Flores and Wetar islands) and are characterized by normal and normal-oblique slip related to deformation of the subducted slab (Figure 4).

The style of deformation west of 120°E longitude changes compared to the Banda arc collision to the east (Figure 4c). Shallow (0–19.99 km) to intermediate depth (20–39.99 km) events follow the Java trench and are characterized by normal and normal-oblique slip mechanisms related to bending of the Indian oceanic lithosphere as it approaches the trench. North of the trench midcrustal to deep-crustal (40 to 99.99 km) thrust events occur along the main locked part of the plate boundary, while deep focus (>100 km) normal events occur north of the plate interface zone and northward of the island arc within the subducted Indian Ocean slab.

Along the extended margin of western Australia between the northern plate boundary and ~20° south latitude focal mechanisms demonstrate dominantly dextral strike slip or dextral-oblique slip deformation on northeast trending fault planes (Figure 4a) [*Revets et al.*, 2009; *Keep et al.*, 2012]. However, left-lateral, reverse, and normal events also are recorded. For example, the 23 April 1979 M_w 6.2 earthquake (Figure 4a) was interpreted as a left-lateral strike slip event that occurred within the westernmost part (offshore) of Fitzroy trough

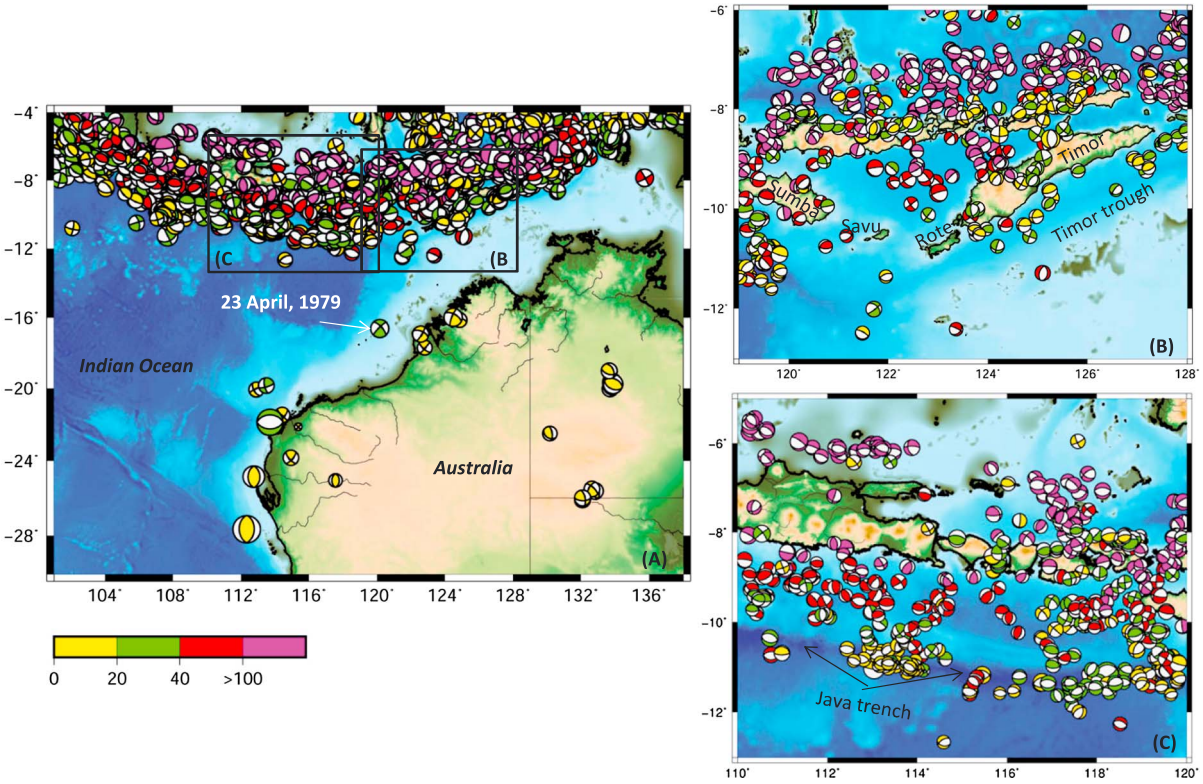

Figure 4. (a) Focal mechanism solutions for the study region. The focal mechanisms are classified based on depth intervals to illustrate the style of faulting within the different structural domains. Note (b) sinistral reverse motion along Timor trough, (c) subduction related pattern along Java trench, and dextral solutions along the western Australia extended margin (Figure 4a) north of 20°S. Centroid moment tensor (CMT) solutions [*Dziewonski et al.*, 1981] are from the CMT project [*Ekström et al.*, 2012; http://www.globalcmt.org/CMTcite.html] for events of $M_w > 5.0$ for the period 1976 onward.

(Figure 1) [*Fredrich et al.*, 1988], a northwest trending failed rift system, rather than along the northeast trending continental margin. Although the available depth resolution is poorly constrained for earthquakes within the Australian continent we infer that these are shallow to intermediate depth (<40 km) events that occur above the Moho within the continental lithosphere.

The islands of Sumba, Savu, and Rote align with the northwestern most margin of the Australian continental plate (Figures 1, 2, and 4b) and are emerging and internally deforming as a result of the collision [*Harris et al.*, 2009; *Roosmawati and Harris*, 2009; *Shulgin et al.*, 2009; *Rigg and Hall*, 2011]. During the past 2 Ma, pelagic deposits from the offshore areas of Rote and Savu have been uplifted along large-scale thrusts at rates of ~1.5 and 2.3 mm yr^{-1}, respectively [*Roosmawati and Harris*, 2009]. Sumba, Savu, and Rote also are moving in a 011°E to 015°E direction, but at 23 to 32 mm yr^{-1} (relative to a fixed Sunda Shelf reference frame) [*Harris et al.*, 2009; *Nugroho et al.*, 2009]. This is about one third to one half the velocity of the Australian plate; thus, these islands are partially coupled to the leading edge of the Australian plate. This implies that the remaining two thirds of Australian plate motion is accommodated by distributed deformation on other regional structures. To illustrate the rate of contraction between the Banda arc and Australia, we illustrate selected GPS station velocities relative to fixed Australia reference frame (Figure 2) [*Nugruho et al.*, 2009], which show that Timor, Rote, Suva, and Sumba are colliding with Australia at a rate of 24 to 39 mm/yr. The collision also is causing regional downwarping of the northern ~500 km of the Australian plate [*Langhi et al.*, 2011], recognizable by the giant 500 km wide continental shelf [*Bourget et al.*, 2012], sinuous shoreline morphology (Figure 1), drowned Last Interglacial reef deposits [*Collins*, 2002], and submerged sea level lowstand coastal landforms and deposits (Figure 5) [*Hengesh et al.*, 2011].

Geomorphic and stratigraphic observations provide constraints on subsidence rates in Browse and Roebuck basins. Scott Reef and Rowley Shoals are atolls located on the outermost continental shelf that have formed through long-term crustal subsidence (Figure 1). Drilling, sampling, and dating programs at Scott Reef and

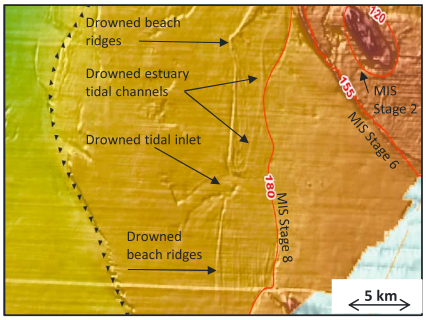

Paleo sea level indicator elevations used on sea level prediction plot

Marine Isotope Stage (MIS)	Formation Elevation (m)	Current Elevation (m)	Elev. Difference (m)	Age (Ka)	Subsidence Rate mm/yr
2	-120	-125	-5	18	-0.28
5e*	5.5	-30	-35.5	125	-0.28
6	-128	-155	-27	137	-0.20
8	-108	-180	-72	250	-0.29

* = 5e elevation reported by Collins, 2002 from Scott Reef.

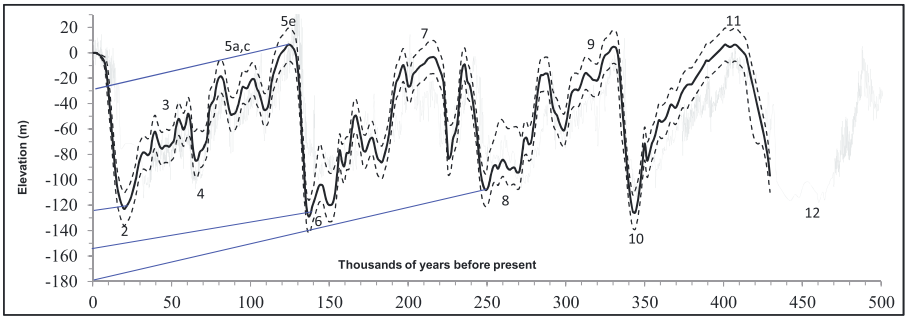

Figure 5. Sea level prediction curves and estimated subsidence rates for submergent estuarine features and strand lines in northern Browse basin [*Hengesh et al*., 2011]. Depth and age of MIS 5e from Scott Reef [*Collins*, 2002] provide baseline subsidence curve. Solid black curve and dashed uncertainty bands from *Waelbroeck et al*. [2002] and grey curves from *Rohling et al*. [2009].

Rowley Shoals, identified marine isotope stage (MIS) 5e corals (~125 ka) at −30 m and −27 m elevations, respectively [*Collins*, 2002; *Collins and Testa*, 2010]. The age and elevation of these corals yield a subsidence rate of −0.28 mm yr^{-1} at Scott Reef and −0.2 mm yr^{-1} at Rowley Shoals. Marine geomorphological investigations in Browse basin also identified submergent strandlines, lowstand beach ridges, and estuarine tidal channel features at −180 m, −155 m, −30 m, and −125 m depths (Figure 5) [*Hengesh et al*., 2011].

We used a sea level fluctuation curve [*LaJoie et al*., 1991] to calculate subsidence rates for submergent shoreline features in northern Browse basin. The subsidence rates were calculated using the MIS 5e sea level elevation data for Scott Reef [*Collins*, 2002] to establish a baseline subsidence rate. The sea level fluctuation curve demonstrates that the observed submerged shoreline features correlate to marine isotope stages 8, 6, 5, and 2 and are consistent with subsidence rates of 0.2 to 0.29 mm yr^{-1} (Figure 5).

A system of faults follows the offshore continental margin of western Australia (Figure 1). The faults extend 1400 km southward, from the intersection of the extended continental margin with the northern plate boundary east of Scott Plateau, to the Cape Range. These structures display evidence of late Neogene to Quaternary deformation [*Keep and Moss*, 2000] including folding and faulting of the seafloor and shallow subbottom sediments [*Simpson and Cooper*, 2008]. A zone of deformation then continues onshore for an additional 600 km [*Whitney and Hengesh*, 2015a, 2015b; *Whitney et al*., 2015].

3. Active Tectonic Structures Along Australia's Western Passive Margin

We have interpreted 2-D and 3-D seismic data from Browse, Roebuck, and Northern Carnarvon basins (Figure 1) to assess the characteristics of post Neogene intraplate deformation along the rifted continental margin of western Australia, south of the northern plate boundary (Figure 6). We use the Geoscience Australia Browse Basin High Resolution (BBHR) 2-D survey data to provide basin-wide coverage and 3-D data to illustrate more detailed characteristics of faulting within northern Browse basin (see box on inset of Figure 1). The Geoscience Australia data release [*Cortese et al*., 2014] also was used to assess faulting within the Roebuck and northern Carnarvon basins. We focused on assessing deformation above the late Miocene horizon, which is consistent with the Pliocene to Holocene interval in Browse basin [*Simpson and Cooper*, 2008], and the late Miocene in the Roebuck and Carnarvon basins [*Cortese et al*., 2014]. This

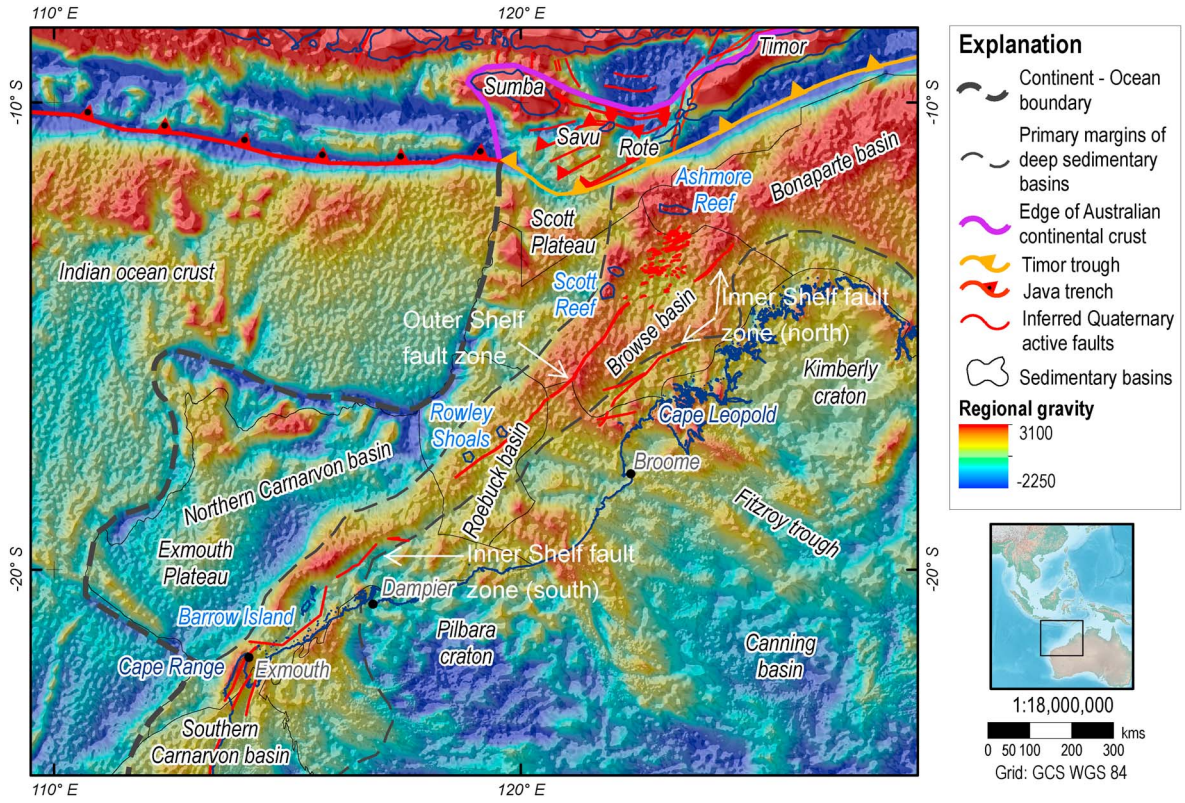

Figure 6. Merged free-air and isostatic gravity anomalies and inferred Quaternary active faults along the western margin of Australia [*Geoscience Australia*, 2009]. Note the association of faults with areas of high gravity anomaly associated with former rift margin basins.

section was selected as its age corresponds to the timing of the onset of collision along the Sumba, Savu, and Rote islands part of the northern plate boundary [*Roosmawati and Harris*, 2009] and eliminates potential confusion with earlier Neogene reactivation [*Keep et al*., 2007; *Keep and Harrowfield*, 2008] and rift era structures [*Cathro and Karner*, 2006].

We discuss three primary zones of faulting. From north to south these include the following: the Inner Basin fault zone, a dense zone of seafloor faults within northern Browse basin; the Outer Shelf fault zone, a transcurrent zone of faults along the outer continental shelf that extends from Scott Reef to Rowley

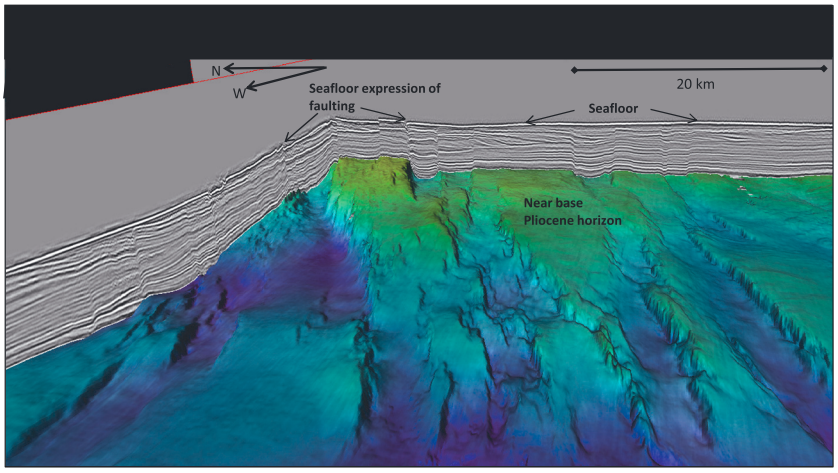

Figure 7. Perspective view to northeast across North Browse 3-D survey showing faulting of a horizon near the base of the Pliocene section. See box on inset of Figure 1 for location.

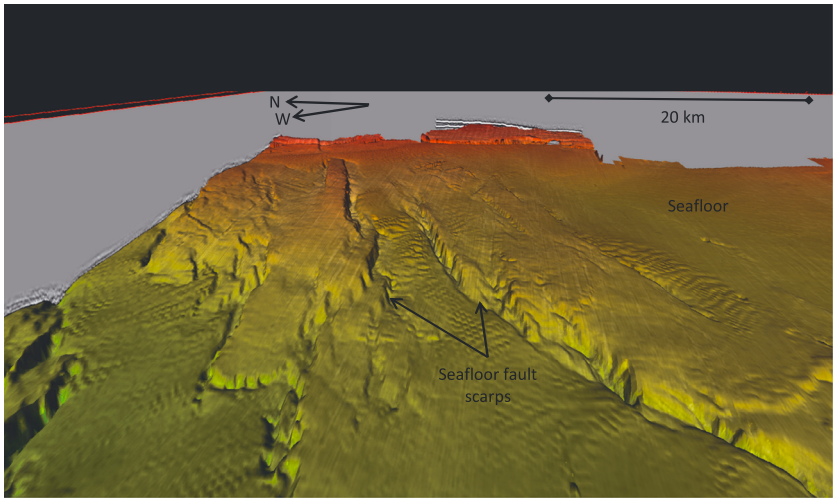

Figure 8. Perspective view to northeast across North Browse 3-D survey showing faulting of seafloor horizon. See box on inset of Figure 1 for location.

Shoals; and the Inner Shelf fault zone, a zone of shorter less continuous transcurrent faults that extend along the inner continental shelf from northeastern Browse basin to the area offshore of Dampier peninsula (Figure 1). Figure 6 shows the faults superimposed on the merged free-air and isostatic gravity anomaly map [*Geoscience Australia*, 2009] for western Australia and the eastern Indian Ocean. The gravity data illustrate the location and extent of the Paleozoic and Mesozoic age basins that compose the Westralia Superbasin of *Yeates et al*. [1987] along the former rifted margin. The steep anomaly gradients along the southeast and northwest sides of the basins are inferred to coincide with the main structures controlling the basin margins (i.e., basin bounding faults). The faults on the inner continental shelf follow the major gravity anomalies that coincide with the eastern margin of the rift basins. The Outer Shelf fault zone

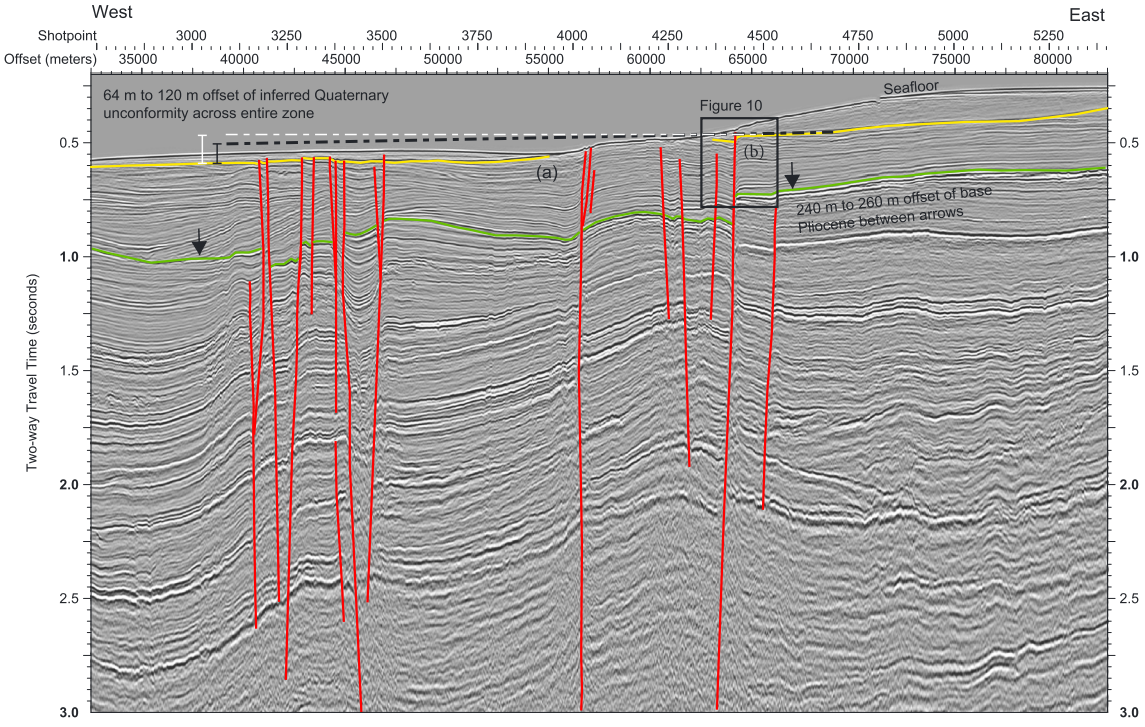

Figure 9. Portion of seismic line BBHR-11 showing faulting of the base of Pliocene and Quaternary unconformities and present-day seafloor northeast of Scott Reef in Browse Basin. See Figure 1 for location. Offsets measured between black arrows. Vertical scale in two-way time (seconds).

Table 2. Summary of Displacement Measurements From Inner Basin Fault Zone on Seismic Line BBHR-11[a]

Figure	Horizon	Zone of Deformation	Width of Zone (m)	Throw (s TWT)		Displacement (m)	
				Minimum	Maximum	Minimum	Maximum
Figure 9	Base Pliocene	Entire fault zone	30,000	0.30	0.325	240.0	260.0
Figure 9	Quaternary unconformity	Entire fault zone	30,000	0.08	0.15	64.0	120.0
Figure 10	Quaternary unconformity	Individual fault strand	500	0.019	0.028	15.2	22.4
Figure 10	Seafloor (late Quaternary)	Individual fault strand	500	0.0060	0.0068	4.6	5.2

[a]Displacement calculated using seismic velocity of 1600 m/s for shallow section (late Miocene to seafloor); seafloor offsets measured assuming a seawater velocity of 1540 m/s.

follows the axes of the basins (Figure 6) and aligns with the continental shelf break between Scott Reef and Rowley Shoals.

3.1. Inner Basin Fault Zone

The North Browse 3-D survey overlies the northeastern part of the Inner Basin fault zone (inset in Figure 1), a 50 km wide by 100 km long zone of N70°E to N80°E trending faults that extends across northern Browse basin. The fault zone forms a cluster of horsts and grabens that deform Pliocene and Quaternary deposits and the seafloor. Figure 7 is a view to the northeast across the 3-D survey area that illustrates the pattern of faulting across a horizon near the base of the Pliocene section, and Figure 8 illustrates deformation of the seafloor in the same area. The individual faults are up to 75 km long, vertical to subvertical, and produce alternating normal and reverse displacement along strike. The same zone of deformation was observed along 2-D seismic line BBHR-11 (Figure 9).

At the location of BBHR-11 (Figure 1), the fault zone is approximately 27 km wide with multiple subparallel fault splays. There is an overall down-to-the-northwest sense of vertical deformation indicated by offset of the base Pliocene and inferred Quaternary horizons (Figure 9). The green horizon marks the stratigraphic position of the base of the undifferentiated Pliocene to Holocene interval defined by *Simpson and Cooper* [2008]. The yellow horizon indicates the position of an unconformity in the upper part of the Pliocene to Holocene section [*Simpson and Cooper*, 2008], which is inferred to be of Quaternary age.

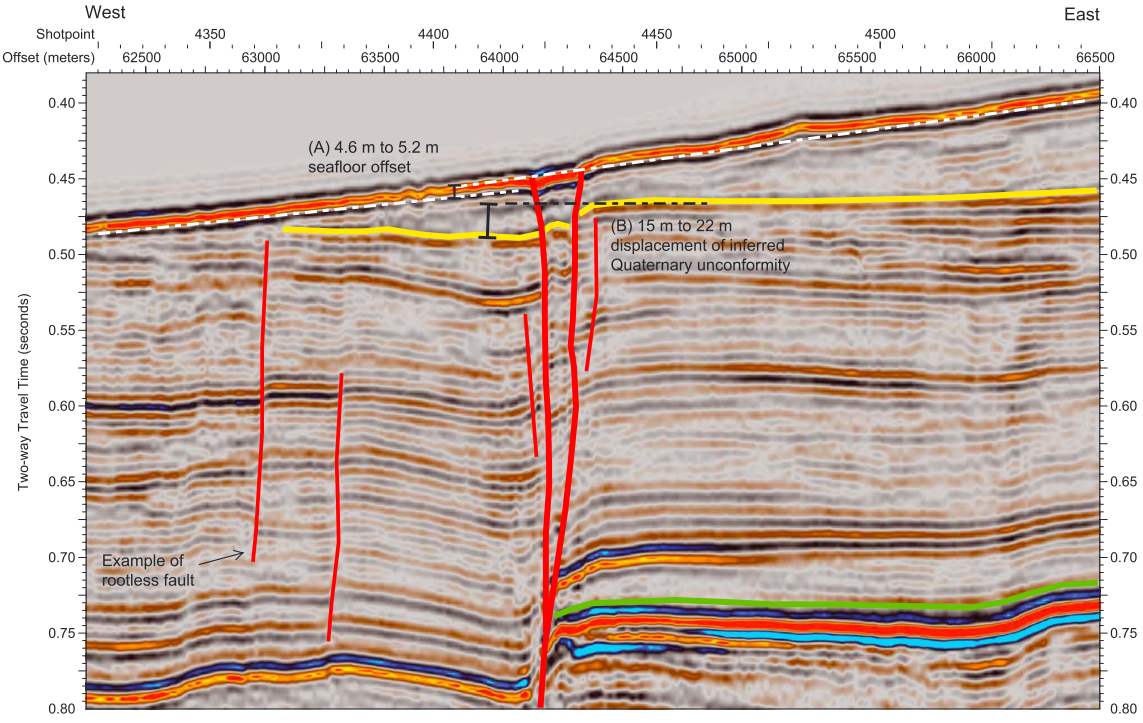

Figure 10. Enlargement showing shallow faulting along BBHR-11 where it crosses the Inner Basin fault zone. Note offset of seafloor (A) and inferred Quaternary unconformity (B) across fault splays. Unconformity at the base of Pliocene section faulted down to the west and out of view. Vertical scale in two-way time (seconds).

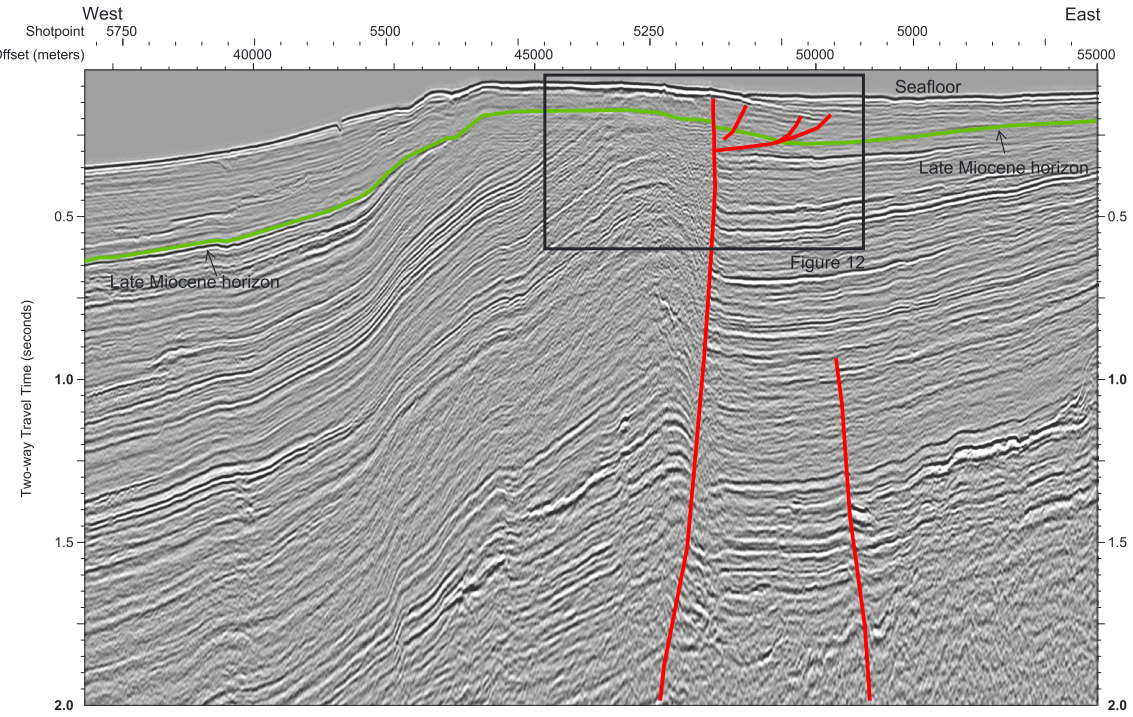

Figure 11. Example of transpressional faulting from BBHR-01 along Barcoo fault section [*Keep and Moss*, 2000] of the Outer Shelf fault zone north of Rowley Shoals. Vertical scale in two-way time (seconds). Location shown in Figure 1.

The base Pliocene horizon (Figure 9) is offset by faults that have produced 0.300 to 0.325 s two-way travel time (TWT) (240 to 260 m assuming 1600 m/s *p* wave velocity) cumulative down-to-the-northwest vertical displacement (Table 2). The faults extend upward through the section and have produced 0.08 to 0.15 s TWT (~64 to 120 m) cumulative down-to-the-west vertical displacement of the inferred Quaternary unconformity in the upper part of the Pliocene to Holocene section. Displacement of the inferred Quaternary unconformity across one of the individual fault strands (Figure 10) is approximately 0.019 to 0.028 s TWT (15 to 22 m). Displacement of the seafloor across the same fault strand is 0.006 to 0.0068 s TWT (4.6 to 5.2 m assuming a seawater velocity of 1540 m/s). Although there is an overall down-to-the-northwest sense of displacement, the sedimentary sequences and unconformities between individual fault strands within the Inner Basin fault zone are anticlinally folded. The inferred Quaternary unconformity between points (a) and (b) on Figure 9 has been eroded from the top of the fold.

The Inner Basin fault zone extends across northern Browse basin from the northeastern part of the basin near the Browse-Bonaparte transition southwestward toward Scott Reef (Figure 1). This zone of deformation intersects the northern end of the Outer Shelf fault zone southeast of Scott Reef.

3.2. Outer Shelf Fault Zone

The Outer Shelf fault zone initiates at the southern end of the Inner Basin fault zone in the central Browse basin and extends approximately 500 km to the southwest (Figure 1). The fault extends from an area approximately 30 km southeast of Scott Reef to 13 km east of Imperieuse Reef, the southernmost of the Rowley Shoals (Figure 6). The N70E° to N80°E trending faults of the Inner Basin fault zone transition to the N35°E to N50°E trend of the Outer Shelf fault zone (Figure 6). The Outer Shelf fault zone consists of two sections. The northern section is approximately 280 km long and bounds the east side of an ~ 200 km long anticline, referred to in petroleum exploration literature as the Barcoo fault and Lynher structure [*Struckmeyer et al.*, 1998; *Keep and Moss*, 2000]. The southern section of the Outer Shelf fault zone is approximately 220 km long and extends from the southern end of the northern fault section to Rowley Shoals. The Rowley Shoals are a series of atolls, similar to Scott Reef, located on the outer continental shelf in the Roebuck Basin (Figures 1 and 6) [*Collins and Testa*, 2010].

Between Scott Reef and Rowley Shoals the fault is expressed as both a fault-bounded fold and a zone of transtensional structures. Approximately 200 km south of Scott Reef, seismic line BBHR-01 (Figure 1) shows that the fault zone dips steeply to the west, extends to the shallow subbottom, and forms an east verging fold

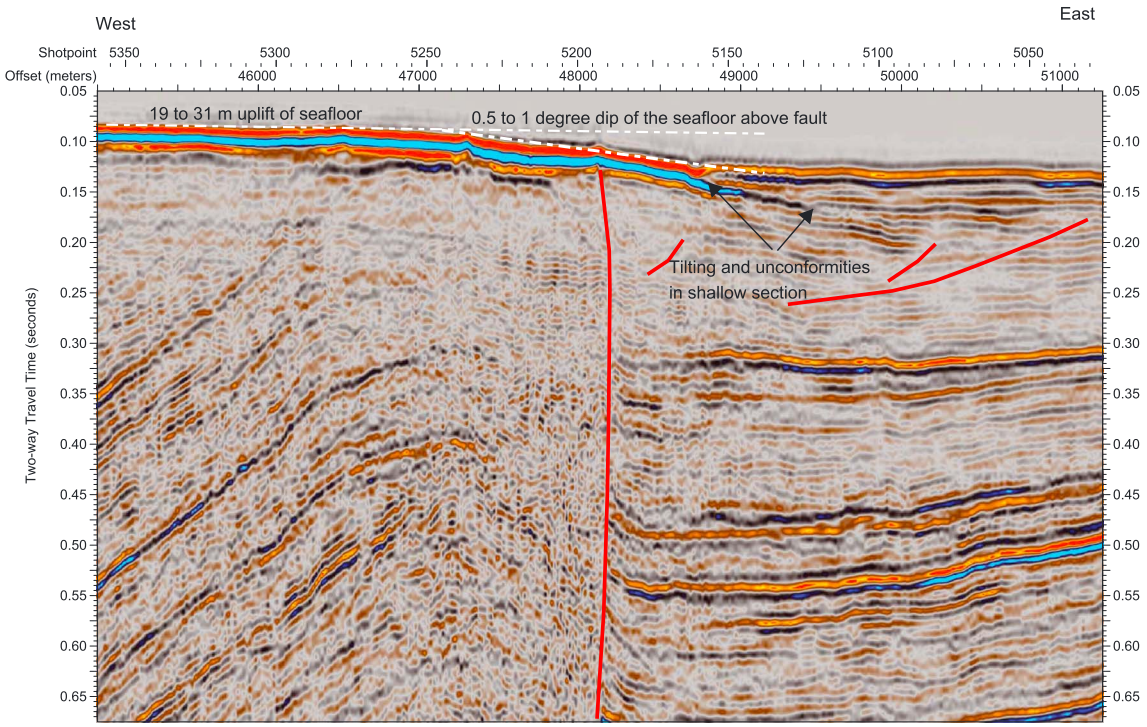

Figure 12. Close-up view of transpressional faulting from BBHR-01 on Outer Shelf fault zone north of Rowley Shoals. Vertical scale in two-way time (seconds). Location of close-up view shown in Figure 11.

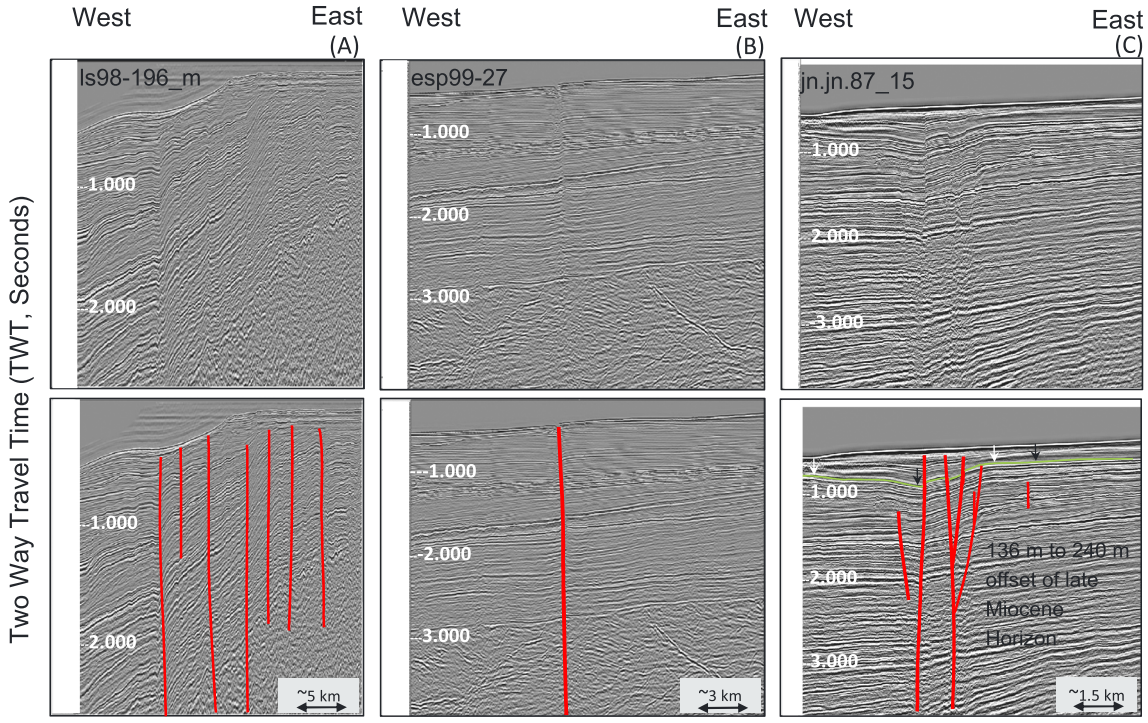

Figure 13. Examples of late Quaternary faulting along the Outer Shelf fault zone near Rowley Shoals. Styles of deformation include (a) transpressional, (b) dominantly transcurrent, and (c) transtensional with negative flower structure. (top row) Uninterpreted and (bottom row) interpreted. Vertical scale in two-way time (seconds). Location shown in Figure 1. White and black arrows shown in Figure 13c (bottom) illustrate locations where minimum and maximum offset measurements were taken on late Miocene unconformity.

Table 3. Summary of Displacement Measurements Across Seismic Line BBHR-01 on Outer Shelf Fault Zone

			Throw (s TWT)		Displacement (m)	
Figure	Horizon	Zone of Deformation	Minimum	Maximum	Minimum	Maximum
Figure 12	Seafloor (late Quaternary)	Fault on east side of east verging anticline	0.025	0.04	19.3	30.8
Figure 13	Late Miocene	Fault-bounded graben; negative flower structure	0.17	0.30	132.0	240.0

on the hanging wall side of the fault (Figure 11). The seabed is tilted approximately 0.5° to 1.0° to the east (against the 0.5° to 1.0° westward gradient of the continental shelf) with 0.025 to 0.04 s TWT (19 to 31 m) uplift or warping of the seabed across the fold (Figure 12). The uplift has produced at least two erosional unconformities directly beneath the seabed pulse that starts at the slope inflection (Figure 12). West dipping subsidiary thrusts deform the shallow section on the east side of the fault.

The Outer Shelf fault zone changes expression from transpressional to transtensional styles of deformation along strike. Near Rowley Shoals (Figure 6) the fault is expressed as a ~15 km wide zone with multiple fault strands that have a normal, down-to-the-west sense of deformation (Figure 13a), a single near-vertical fault strand (Figure 13 b), and a ~5 km wide negative flower structure (Figure 13c). The fault geometry and sense of displacement are consistent with transtensional, transcurrent, and transpressional deformation. Near the southern end of the fault zone, south of Rowley Shoals, the fault has locally produced 0.17 to 0.3 s TWT (136 to 240 m) down-to-the-west displacement of the late Miocene horizon across a series of fault splays that form a negative flower structure and extends to the shallow subbottom just beneath the seafloor (Table 3 and Figure 13c).

3.3. Inner Shelf Fault Zone

The Inner Shelf fault zone extends along the eastern side of the Browse and Carnarvon basins (Figure 6). The faults follow gravity anomalies on the eastern basin margins (Figure 6) but are less continuous than structures along the Outer Shelf fault zone. Fault segments are observed extending between 60 and 180 km in length.

Seismic line BBHR-04 crosses multiple fault strands across an approximate 40 km wide deformation zone (Figure 14). The western strand of the fault zone (Figure 15) dips steeply to the east and produces a down-

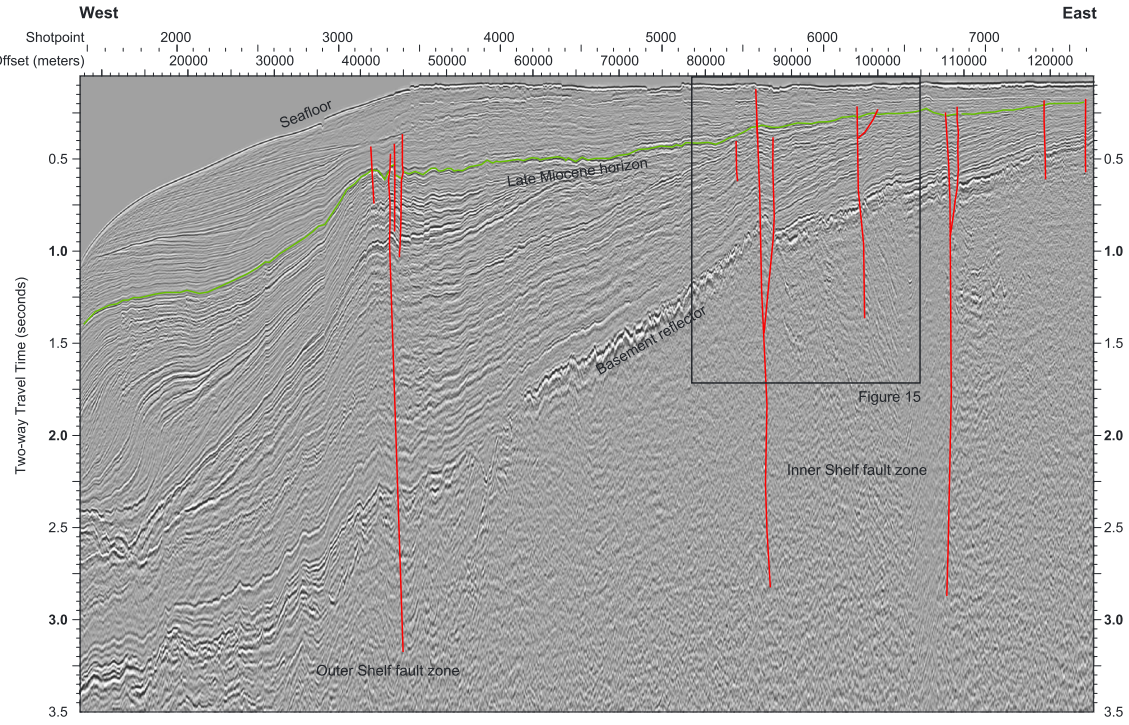

Figure 14. Portion of seismic line BBHR-04 showing faulting of the late Miocene to Quaternary unconformities and present-day seafloor along the Inner Shelf fault zone. Vertical scale in two-way time (seconds). Location shown in Figure 1.

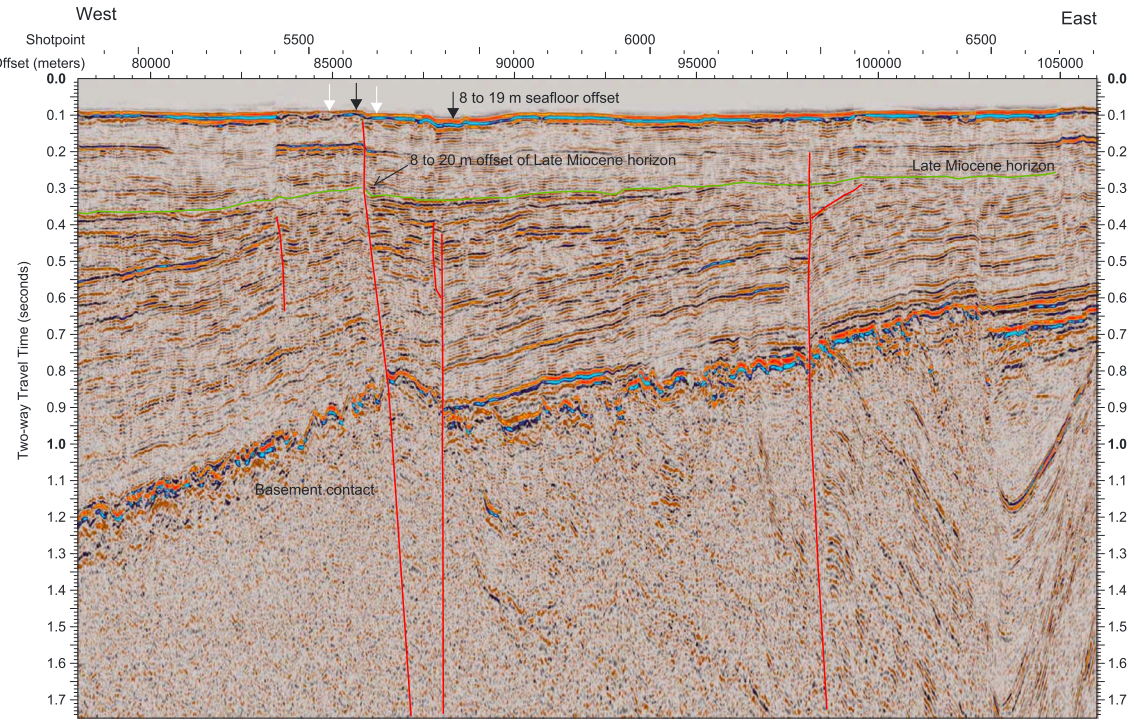

Figure 15. Close-up of seismic line BBHR-04 showing faulting of the late Miocene to Quaternary unconformities and present-day seafloor along the Inner Shelf fault zone. Vertical scale in two-way time (seconds). Location shown in Figure 14. White and black arrows illustrate locations of minimum and maximum offset measurements for both seafloor and late Miocene unconformity.

to-the-east displacement of the basement contact as well as an east facing scarp on the seafloor. This fault strand has two splays that converge at depth near the basement contact. The green horizon marks the approximate position of a late Miocene unconformity, which is overlain by Pliocene to Quaternary deposits. The stratigraphic section between the late Miocene horizon and the seafloor has been anticlinally folded across the western strand. The fault has produced 0.01 to 0.025 s TWT (8 to 19 m) up-on-the-west seafloor displacement (Table 4). Offset of the late Miocene horizon across the western strand of the fault ranges from 0.01 to 0.025 s TWT (8 to 20 m). The fold across the late Miocene unconformity has an amplitude of 0.04 to 0.045 s TWT (32 to 36 m). The eastern strand dips vertically and has a subsidiary west dipping fault splay that locally has tilted and folded the section adjacent to the fault.

The Inner Shelf fault zone continues southward along the eastern basin margin offshore of Dampier peninsula (Figure 6). This section of the fault is 180 km long, 12 km wide, and trends in an N50°E direction. The northern end of this fault segment bends to a N90E direction and has a normal component of motion that displaces the late Miocene horizon and the overlying Quaternary section (Figure 16 and Table 4). This fault segment (observed on line s136_136_24) has produced 0.15 to 0.18 s TWT (120 to 144 m) of down-to-the-north displacement of the late Miocene horizon, 0.015 to 0.018 s TWT (11.8 to 14.3 m) of down-to-the-north displacement of a ~500 Ka Quaternary horizon [*Gallagher et al*., 2014], and 0.039 to 0.041 s TWT (30.8 to

Table 4. Summary of Displacement Measurements Across Seismic Line s136_136_24_mig_time on the Southern Part of the Inner Shelf Fault Zone

			Throw (TWT, s)		Displacement (m)	
Figure	Horizon	Zone of Deformation	Minimum	Maximum	Minimum	Maximum
Figures 16 and 17	Late Miocene	Entire fault zone	0.15	0.180	120.0	144.0
Figure 17	500 ka	Entire fault zone	0.015	0.018	11.8	14.3
Figure 17	1.0 Ma	Entire fault zone	0.039	0.041	30.8	32.5

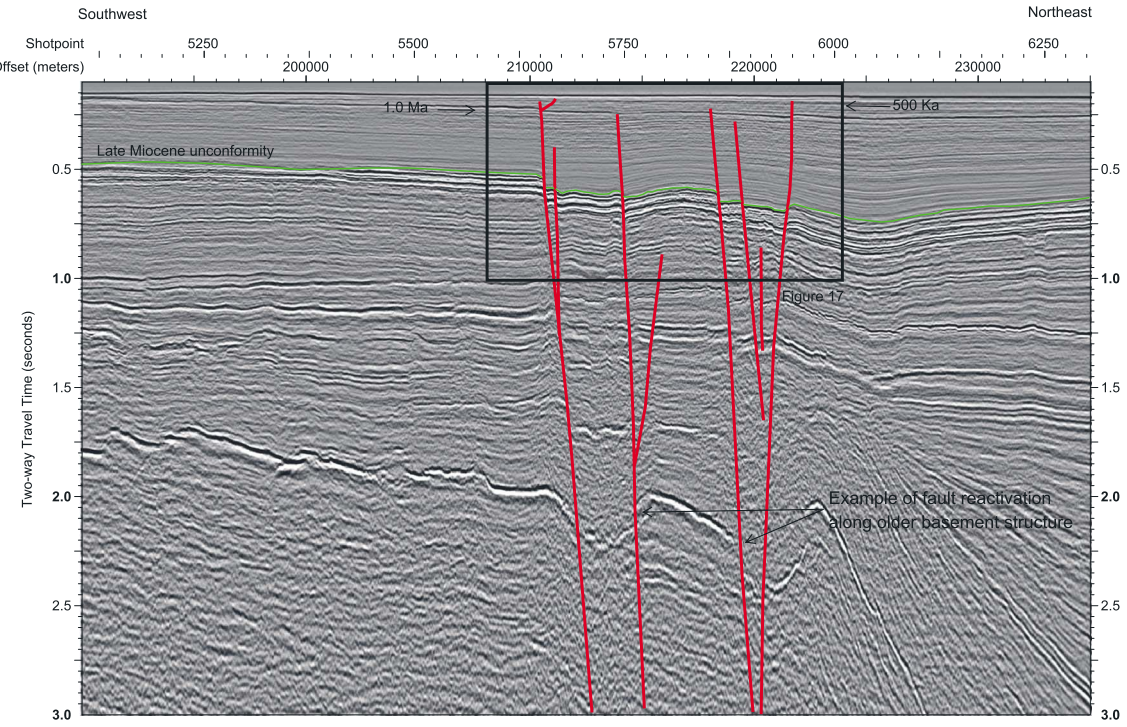

Figure 16. Portion of seismic line s136_136_24 showing faulting of the late Miocene unconformity and Quaternary deposits [*Gallagher et al.*, 2014] along the Inner Shelf fault zone, offshore Dampier. Vertical scale in two-way time (seconds). Location shown in Figure 1.

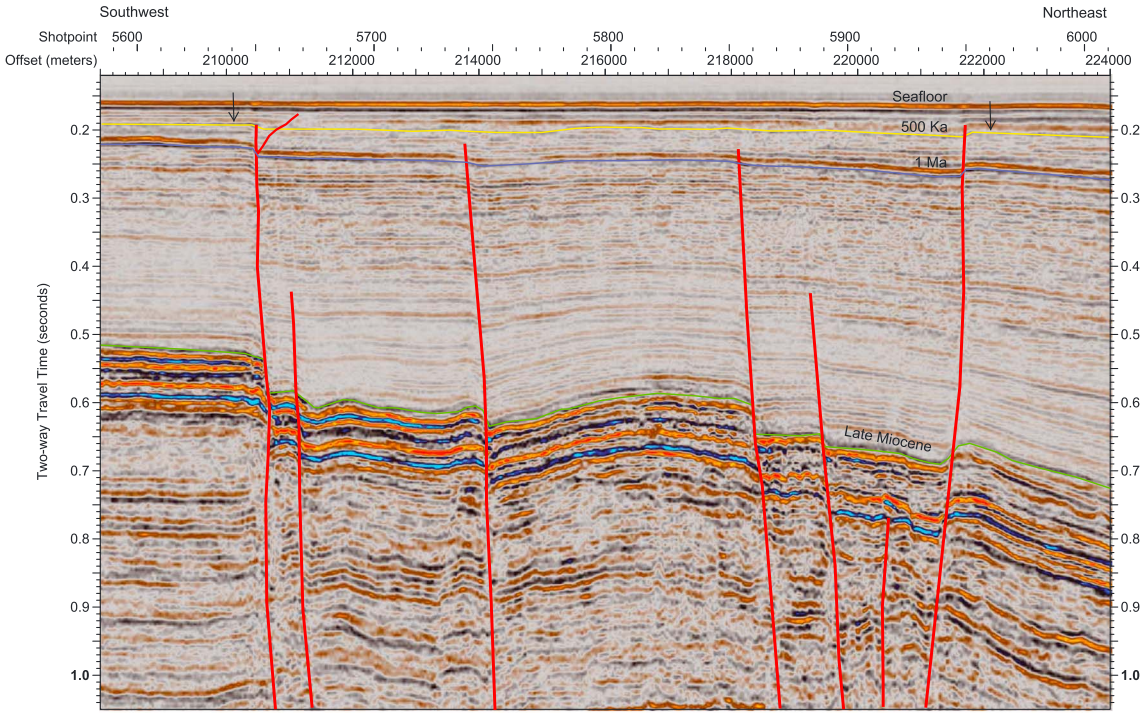

Figure 17. Close-up of faulting of the Pliocene and Quaternary deposits [*Gallagher et al.*, 2014] along the southern part of the Inner Shelf fault zone, offshore Dampier. Portion of seismic line s136_136_24. Vertical scale in two-way time (seconds). Location shown in Figure 1.

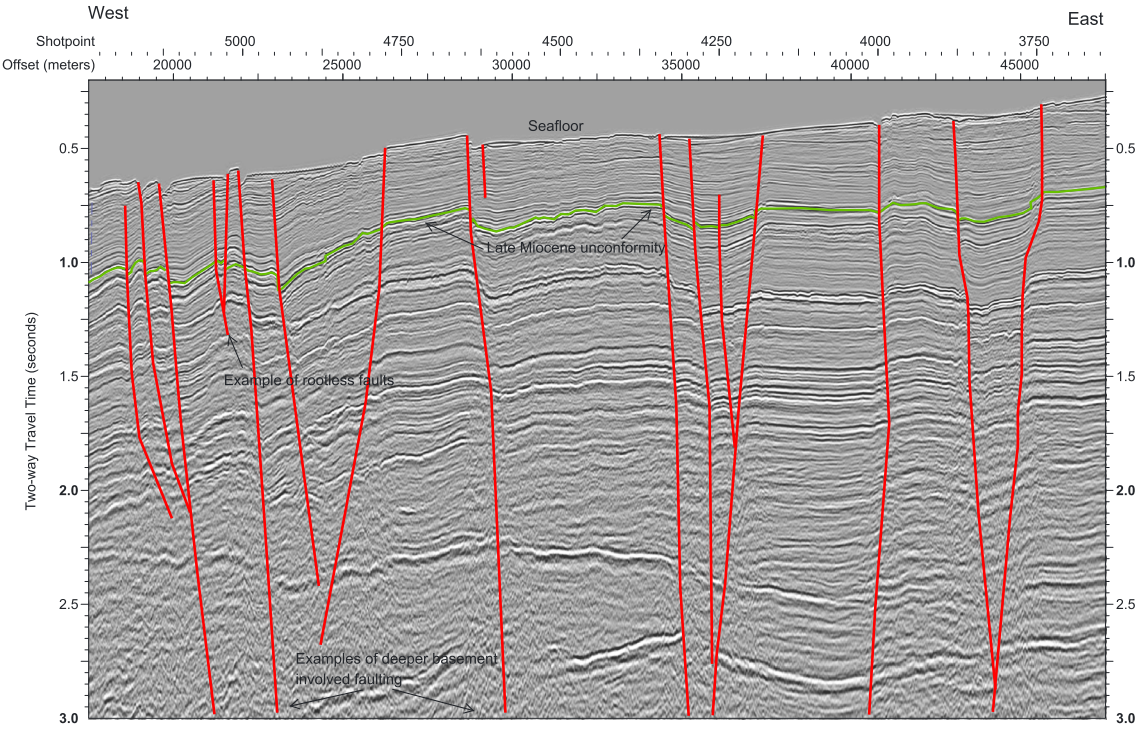

Figure 18. Seafloor faulting on 2-D line BBHR-12 across northern Browse basin illustrating both deep seated (possibly seismogenic) and rootless (aseismic) faults within the Inner Basin fault zone. Vertical scale in two-way time (seconds). Location shown in Figure 1.

32.5 m) of down-to-the-west displacement of a ~1.0 Ma Quaternary horizon (Figure 17). The seabed is not deformed, but the water depth at the location of the fault is only ~96 m, so this part of the continental shelf would have been abraded through current and wave action during multiple Pleistocene sea level lowstands. The fault zones on the continental shelf continue southward as the Flinders-Scholl Island fault zone (B. B. Whitney et al., Styles of fault reactivation within a formerly extended continental margin, North West Shelf, Australia, submitted to *Tectonophysics*, in revision, 2015).

4. Discussion

4.1. Style and Rates of Shallow Faulting in the Western Australia Shear Zone

Geophysical data collected along the North West Shelf image a 1400 km long northeast trending system of late Neogene to Quaternary active faults that follow the former rifted continental margin of western Australia from Ashmore Reef southward to the Cape Range (Figures 1 and 6). This fault system is referred to as the Western Australia Shear Zone [*Whitney et al.*, 2014; *Whitney*, 2015]. In the Browse and Roebuck basins, there are two subparallel zones of faults that trend along the inner (eastern) and the outer (western) parts of the continental shelf; these are referred to as the Inner Shelf and Outer Shelf fault zones, respectively. Focal mechanism solutions along the fault system indicate a dextral strike slip sense of motion (Figure 4). Seismic data show that within both the Inner and Outer Shelf fault zones individual fault strands can have both normal and reverse components of secondary deformation (Figures 11 and 13) that are kinematically related to restraining and releasing bends or step overs along fault strike. Some fault strands within these zones are observed on seismic sections to be associated with older basin bounding structures (Figures 16 and 18) and follow the basin margins identified on the gravity anomaly maps (Figure 6). These faults extend to basement depth and are inferred to be potentially significant seismogenic sources. Another set of faults deform the shallow section but are rootless (Figures 10 and 18). The shallower faults are interpreted to be either bending moment faults responding to folding at depth or shallow accommodation structures (such as Riedel shears) that are responding to differential motion between adjacent fault blocks (Figures 15 and 18). Due to the shallow depth and limited potential rupture dimensions, these shallow faults are not likely to be significant seismogenic sources, but rather secondary structures indicative of crustal strain associated with activity along nearby larger structures.

The Inner Basin fault zone is interpreted to represent the northern segment of the Western Australia Shear Zone. The fault zone trends ~N70°E to N80°E obliquely across the Browse basin (Figures 1 and 6) and extends between the northern part of the Outer Shelf and the northern Inner Shelf fault zones. The style of vertical deformation within the zone is characterized by steeply dipping faults that bound alternating horsts and grabens (Figures 7 and 8). We infer that the Inner Basin fault zone represents a major segmentation point along the Western Australia Shear Zone base on the following observations: (a) there is a large change in fault orientation from ~N70°E to N80°E (Inner Basin fault zone) to ~N35°E to N50°E (Inner Shelf and Outer Shelf fault zones), (b) the styles of faulting change from contractional or transpressional deformation along the northern section of the Outer Shelf fault zone to extensional or transtensional deformation along the Inner Basin fault zone, and (c) the pattern of faulting changes from a discrete through going fault (Outer Shelf fault zone) to a >50 km wide zone of deformation along the Inner Basin fault zone. This segmentation point lies approximately 35 to 40 km east-southeast of Scott Reef (Figure 1). The faulting pattern and style of deformation along the Inner Basin fault zone are compatible with both a right releasing bend or step over between the Outer Shelf and Inner Shelf fault zones and the warping and flexure occurring along the northern part of the North West Shelf.

The transtensional parts of the Outer Shelf fault zone have a down-to-the-west component of vertical displacement (Figures 9 and 18). We use the approximate base of the Pliocene to Holocene section [*Simpson and Cooper*, 2008], inferred Quaternary unconformities, middle to late Quaternary horizons [*Gallagher et al.*, 2014], and the seabed to estimate rates of vertical deformation (Table 5). Minimum slip rates are calculated by dividing the minimum displacement by the maximum age, and the maximum slip rate is calculated by dividing the maximum displacement by the minimum age. In computing these rates we make the following assumptions:

1. In Browse basin, we use geomorphological observations to constrain the age of the seafloor reflector. Our analysis of submergent shoreline features observed on the seafloor [*Hengesh et al.*, 2011] suggests these features correlate to MIS 8, 6, and 2 (Figure 5). For our slip rate analyses we apply the geomorphically constrained ages of 250,000 and 125,000 years to approximate the age of the seafloor reflector but acknowledge the uncertainty in this approach.
2. In the Carnarvon and Roebuck basins, 0.5 and 1.0 Ma reflectors have been identified in the shallow section [*Gallagher et al.*, 2014]. We directly compute slip rates based on the age and offsets of these horizons.
3. The age of onset of regional tectonic deformation ranges from 1 to 3 Ma, consistent with the timing of the collision along the Sumba-Savu-Rote ridge [*Roosmawati and Harris*, 2009; *Rigg and Hall*, 2011]. We use the age of onset of the collision and measured offsets of the late Miocene horizons to estimate the long-term Plio-Pleistocene rates of deformation.

The vertical slip rates across a 27 km wide section of the Inner Basin fault zone (Figure 9) are estimated based on offsets of the base of the Pliocene to Holocene section [*Simpson and Cooper*, 2008] and an inferred Quaternary unconformity (Table 5). The estimated vertical slip rates range from 0.06 to 0.26 mm/yr. The estimated vertical slip rates across one of the individual fault strands (measured a distance of 500 m across the fault zone) for the seafloor and inferred Quaternary horizon range from 0.02 to 0.04 mm/yr. The slip rates based on offsets of the inferred Quaternary unconformity and the Pliocene to Holocene section are in good agreement, as are the rates based on offsets of the seafloor and the inferred Quaternary unconformity for the individual fault trace (Table 5 and Figures 9 and 10). We infer, based on the position of some upward fault terminations within the lower Pliocene section, that deformation along the continental shelf had begun by the early to middle stages of the collision along the Sumba-Savu-Rote ridge [*Roosmawati and Harris*, 2009; *Rigg and Hall*, 2011].

The maximum estimated vertical tectonic slip rates across the Inner Basin fault zone approximate the subsidence rates of ~0.28 mm/yr at Scott Reef [*Collins and Testa*, 2010] on the western side of the Outer Shelf fault zone (Figure 5). This indicates that the subsidence of the outer continental shelf, and Quaternary submergence of Scott Reef, is at least partly related to the overall down-to-the-west pattern of tectonic deformation occurring along the Inner Basin fault zone. An additional component of vertical deformation may be caused by regional downwarping of the Australian plate as a result of the accretion of the Sumba to Timor section of the Banda arc onto the northern Australian continental shelf [*Audley-Charles*, 2004, 2011; *Duffy et al.*, 2013].

The style of deformation along the northern part of the Outer Shelf fault zone is characterized by faulting along the eastern margin of an east verging anticline (Figure 11). Along seismic line BBHR-01 the seafloor has been uplifted and folded across the anticline (Figure 12). The shallow subbottom stratigraphy has been

AGU Tectonics

10.1002/2015TC004103

Table 5. Estimated Vertical Displacements and Slip Rate Values From Selected Seismic Lines

					Throw (s TWT)		Displacement (m)		Period of Activity (Ma)		Estimated Fault Slip Rate (mm/yr)	
Fault Zone/Seismic Line	Figure	Shot Point Range	Horizon	Zone of Deformation	Minimum	Maximum	Minimum	Maximum	Minimum	Maximum	Minimum	Maximum
Inner Basin fault zone (seismic line BBHR-11)	Figure 9	3125–4600	Inferred Quaternary unconformity	Entire fault zone	0.080	0.150	64	120	0.50	1.00	0.06	0.24
	Figure 9	3125–4600	Base Pliocene	Entire fault zone	0.300	0.325	240	260	1.00	3.00	0.08	0.26
	Figure 10	4410–4450	Seafloor	Individual fault strand	0.006	0.007	5	5	0.13	0.25	0.02	0.04
	Figure 10	4410–4450	Inferred Quaternary unconformity	Individual fault strand	0.019	0.028	15	22	0.50	1.00	0.02	0.04
Outer Shelf fault zone—north section (seismic line BBHR-01)	Figure 12	5250–5175	Seafloor	Fault on east side of east verging anticline	0.025	0.040	19	31	0.13	0.25	0.08	0.25
Outer Shelf fault—south section (seismic line jn.jn.87_15)	Figure 13c	NA	Late Miocene fault offset	Entire fault zone	0.17	0.30	136	240	1.00	3.00	0.05	0.24
Inner Shelf fault zone (north) (seismic line BBHR-04)	Figure 15	5540–5700	Seafloor	Individual fault strand	0.010	0.025	8	19	0.13	0.25	0.03	0.15
	Figure 15	5540–5700	Late Miocene fold amplitude	Individual fault strand	0.040	0.045	32	36	1.00	3.00	0.01	0.04
	Figure 15	5540–5700	Late Miocene fault offset	Individual fault strand	0.010	0.025	8	20	1.00	3.00	0.003	0.02
Inner Shelf fault zone (south) (seismic line s136_136_24_mig_time)	Figure 17	5640–5950	500 ka	Entire fault zone	0.015	0.018	12	14	0.50	0.50	0.02	0.03
	Figure 17	5650–5950	1.0 Ma	Entire fault zone	0.039	0.041	31	32	1.00	1.00	0.03	0.03
	Figures 16 and 17	5600–5975	Late Miocene	Entire fault zone	0.150	0.180	120	144	1.00	3.00	0.04	0.14

Table 6. Summary of Estimated Vertical and Horizontal Slip Rate Values

	Vertical Slip Rate (mm/yr)			Horizontal Slip Rate (mm/yr)		
	Minimum	Average	Maximum	Minimum (1:1 H/V)	Average (5:1 H/V)	Maximum (10:1 H/V)
Inner Basin	0.02	0.14	0.26	0.02	0.70	2.60
Outer Shelf (north)	0.08	0.16	0.25	0.08	0.81	2.46
Inner Shelf (north)	0.03	0.09	0.15	0.03	0.45	1.50
			Average	0.04	0.65	2.2
Outer Shelf (south)	0.05	0.14	0.24	0.05	0.71	2.40
Inner Shelf (south)	0.02	0.08	0.14	0.02	0.40	1.40
			Average	0.03	0.56	1.9

tilted and eroded forming several erosional unconformities that we interpret to represent evidence of late Quaternary fault activity and fold growth. The vertical fault slip rates along the northern part of the Outer Shelf fault zone are estimated based on the amount of seafloor deformation across the fault. The estimated vertical slip rates range from 0.08 to 0.25 mm yr^{-1} (Table 5).

The style of deformation along the southern part of the Outer Shelf fault zone involves dextral transcurrent motion with a down-to-the-west component of vertical displacement. The vertical slip rates along the southern part of the Outer Shelf fault zone near Rowley Shoals are estimated based on offset of the late Miocene horizon [*Cortese et al*., 2014] within a graben located above a negative flower structure (Figure 13c). The vertical slip rates range from 0.05 to 0.24 mm yr^{-1} (Table 5). As with Scott Reef, the maximum estimated vertical slip rates are in close agreement with the measured subsidence rates, about 0.2 mm/yr from last interglacial age corals in the atolls that form Rowley Shoals [*Collins and Testa*, 2010]. This observation suggests that the Quaternary subsidence of Rowley Shoals is related to the overall down-to-the-west pattern of tectonic deformation occurring along the southern part of the Outer Shelf fault zone.

The Inner Shelf fault zone in eastern Browse basin is a basement related dextral transtensional structure with both down-to-the-east and down-to-the-west senses of vertical deformation (Figure 14). At BBHR-04 the fault has produced 8 to 19 m down-to-the-east offset of the seafloor, 8 to 20 m of offset of the late Miocene horizon, and 32 to 36 m folding of the late Miocene horizon (Figure 15). The estimated late Quaternary vertical slip rates range from 0.06 to 0.1 mm yr^{-1} (Table 5).

We did not identify any suitable piercing points with which to assess horizontal slip rates across the fault zones. However, a general indication of horizontal slip rates can be estimated by assuming a range of vertical to horizontal slip ratios. Horizontal to vertical slip ratios for strike slip faults commonly range from 1:1 to 10:1 [*Wells and Coppersmith*, 1994; K. Coppersmith, personal communication, 2015]. We apply these ratios to the minimum, average, and maximum slip rate values for the Inner Basin, Inner Shelf, and Outer Shelf fault zones. The estimated ranges of horizontal slip rate are summarized in Table 6. The estimated horizontal slip rate values in Browse basin therefore range from 0.02 to 2.6 mm yr^{-1}. The estimated horizontal slip rate values to the south in Roebuck basin range from 0.02 to 2.4 mm yr^{-1}. Using the average fault displacements and 5:1 horizontal to vertical slip ratio yields mean estimated horizontal slip rate values of 0.45 to 0.81 mm yr^{-1} for the faults in Browse basin and 0.56 mm yr^{-1} for the faults in Roebuck basin. The range of slip rate values is likely a minimum as we have no data for deformation along faults on Scott Plateau, west of the continental slope.

The down-to-the-west style of faulting produces progressive downwarping of the continental shelf outboard of the fault zones. This downwarping of the shelf explains the presence of both Scott Reef and Rowley Shoals atolls and the anomalously deep continental shelf break that has been observed along parts of the North West Shelf [*Collins and Testa*, 2010]. Submergent strandlines and paleoestuarine deposits are observed to a depth of approximately 180 m below sea level [*Hengesh et al*., 2011], but the shelf break can extend to depths greater than 500 m.

4.2. Neotectonic Framework for Australia's North West Shelf

Three principle tectonic elements define the neotectonic framework of northwestern Australia and influence the internal stability of the central Indo-Australian plate (Figure 19). These elements include the Java trench part of the Sunda Arc, Flores-Wetar thrust and Timor trough part of the Banda collision zone, and the Western

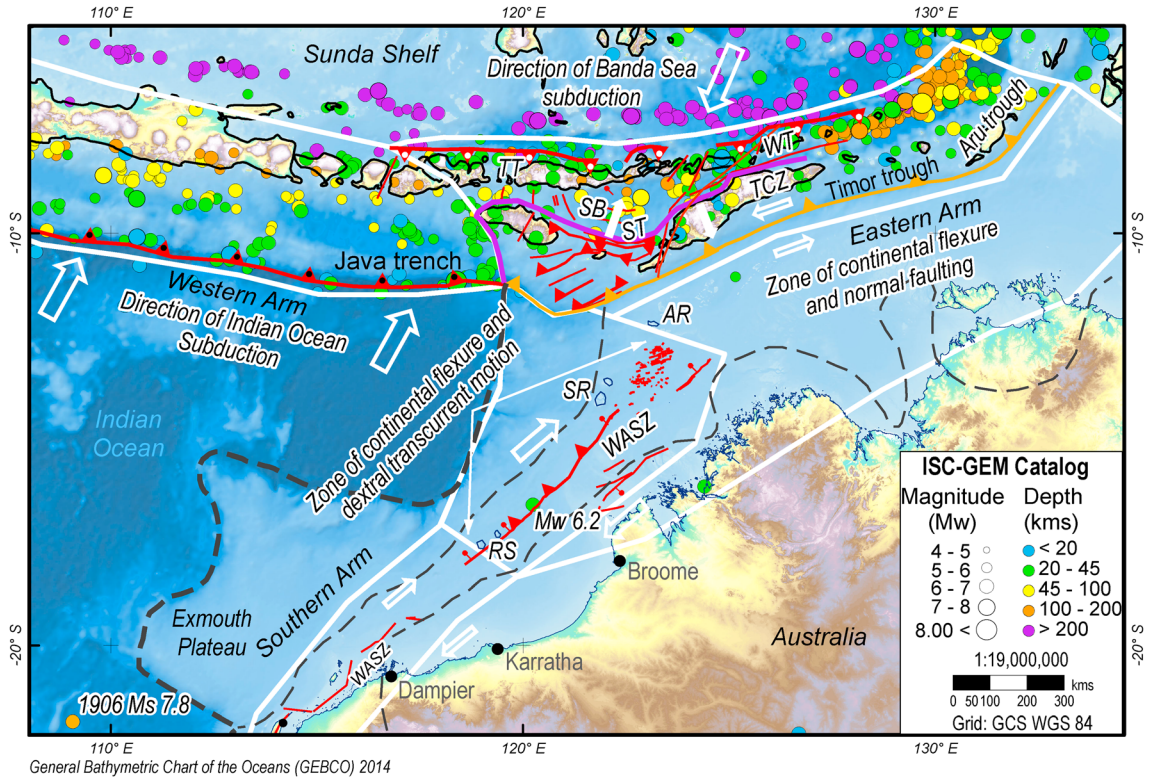

Figure 19. Illustration of major tectonic elements in triple junction geometry: tectonic features labeled per Figure 1; seismicity from ISC-GEM catalog [*Storchak et al.*, 2013]; faults in Savu basin from *Rigg and Hall* [2011] and *Harris et al.* [2009]. Purple line is edge of Australian continental basement and fore arc [*Rigg and Hall*, 2011]. Abbreviations: AR = Ashmore Reef; SR = Scott Reef; RS = Rowley Shoals; TCZ = Timor Collision Zone; ST = Savu thrust; SB = Savu Basin; TT = Timor thrust; WT = Wetar thrust; WASZ = Western Australia Shear Zone. Open arrows indicate relative direction of motion; solid arrows direction of vergence.

Australia Shear Zone. These three tectonic elements intersect near the Ashmore Reef-Savu basin region. Although the Western Australia Shear Zone is a youthful evolving fault system with limited long-term displacement, the kinematic characteristics of the region are consistent with the geometry of a triple junction.

The western arm of the triple junction is defined by the Java trench subduction zone where Jurassic age Indian oceanic crust [*Robb et al.*, 2005] is subducting at a rate of 66 to 72 mm yr^{-1}. The Java subduction zone is characterized by efficient subduction [*Berryman et al.*, 2015; *Pacheco and Sykes*, 1992] of oceanic crust producing a north dipping Benioff zone that extends to more than 640 km depth (Figure 3). The Java subduction zone now terminates at a longitude of approximately 120°E. Type B subduction along the Sunda Arc, and former Banda trench, began about 12 Ma [*Hall*, 2011] and triggered an earlier phase of reactivation along faults on the North West Shelf.

The eastern arm of the triple junction is defined by the south dipping Flores-Wetar thrust and north dipping Timor tectonic collision zone (Figure 19). Together these accommodate south directed subduction of the Banda Sea plate beneath the northern continental margin, as well as south directed back thrusting and obduction of the former Banda subduction zone accretionary prism onto the continental margin [*Audley-Charles*, 2011; *Spakman and Hall*, 2010]. This arm of the plate boundary extends 1200 km eastward along the outer Banda Arc from the termination of the Java trench. The Ashmore Reef to Timor segment of the outer Banda Arc now is undergoing sinistral-oblique deformation related to the highly oblique sense of motion between Australia and Timor. *Nugroho et al.* [2009] measured 24 to 39 mm yr^{-1} south-southwestward motion of Sumba, Rote, and Timor with respect to a fixed Australian reference frame (Figure 2), which is accommodated by thrust and sinistral strike slip faulting (Figure 4). This high rate of deformation is accommodated by numerous structures distributed across the Australian continental shelf, Timor trough, and on the island of Timor [*Duffy et al.*, 2013].

The southern arm of the triple junction, the Western Australia Shear Zone, extends southward from Ashmore Reef to the Cape Range of western Australia (Figure 17) [*Hengesh and Whitney*, 2014; *Whitney and Hengesh*,

2015a, 2015b; *Whitney et al*., 2015; B. B. Whitney et al., submitted manuscript, 2015]. This active fault system (e.g., Inner Shelf and Outer Shelf fault zones) follows the former rifted margin (Figure 6) and affects late Neogene and Quaternary deposits, deforms the continental shelf, and locally offsets the seafloor (Figures 6–18). The Outer Shelf fault zone includes fault segments that extend 800 km southward from Ashmore Reef to Rowley Shoals. This fault zone continues southward to the Flinders-Scholl Island fault zone extending another 600 km to the Cape Range [*Whitney and Hengesh*, 2015a, 2015b]. The 1906 M_s 7.8 Exmouth event occurred in the oceanic basin offshore of the reactivated structures on the former extended margin.

The most significant phase in development of the current tectonic setting was the entry of Australian continental crust into the former Banda subduction zone. Termination of subduction and development of the arc-continent collision began along the eastern part of the Banda arc and migrated westward along the northern plate boundary at a rate of approximately 100 km Ma^{-1} [*Harris*, 1991]. Subduction near Timor ceased about 4 Ma after all oceanic crust was consumed [*Audley-Charles*, 2011]. *Harris et al*. [2009] and *Roosmawati and Harris* [2009] have demonstrated that the collision of the westernmost Australian continental margin with the former Banda trench initiated near Sumba (3–2 Ma), then migrated southeastward to Savu (1.8–0.5 Ma), and then Rote (1.0 Ma to present). Following completion of Type B subduction, the former subduction zone has undergone trench rollback [*Spakman and Hall*, 2010], which is causing southward thrusting of Sumba, Savu, Rote, and Timor over the northern margin of the Australian continental lithosphere [*Harris et al*., 2009; *Rigg and Hall*, 2011]. The ongoing collision on Savu has formed both north and south verging thrusts, has caused uplift of pelagic chalk from depths of $>$2500 m to the surface in less than 1.0 Ma, and has caused emergence of the accretionary prism [*Harris et al*., 2009]. This pattern of deformation demonstrates the high rates of strain at the leading edge of the collision. This collision is reducing the efficiency of northward plate motion at the northwestern corner of Australia compared to the efficient subduction of the Indian Ocean slab along java trench, to the west.

The initiation of subduction about 12 Ma coincided with the initial stage of middle Neogene fault reactivation and basin inversion along Australia's western passive margin [*Australian Geological Survey Organization North West Shelf Study Group*, 1994; *Keep et al*., 1998; *Cathro and Karner*, 2006]. The middle Miocene inversion structures are eroded and overlain by late Neogene erosional unconformities (Figures 9 and 11) indicating a hiatus in deformation along the passive margin between middle Miocene and Pliocene time. The onset of continent-arc collision in the past 3.0 Ma at Scott Plateau [*Roosmawati and Harris*, 2009; *Harris et al*., 2009] occurred once all oceanic crust was consumed along the northern continental margin [*Hall*, 2011; *Audley-Charles*, 2011]. The timing of the collision directly on the rifted margin coincides with the current period of Quaternary activity along Australia's western passive margin. This differential motion is caused by the transition from northward directed subduction of the Indian oceanic crust west of Scott Plateau (120°E), to southward directed subduction along the Flores-Wetar thrust and southward rollback of the former Banda subduction zone at Timor and Rote. We infer that the change in style of collision along the northern plate boundary has created a dextral shear couple across the former passive margin of northwestern Australia and established a triple junction geometry at the apex of three kinematically distinct tectonic elements. The eastern and western arms of this triple junction are active plate boundary elements while the southern arm is an evolving intraplate fault system (Figure 19). The transfer of strain from the plate boundary 1400 km to the south provides a mechanism for deformation within the stable continental region of western Australia and may help explain the large number of neotectonic structures [*Clark et al*., 2012] and elevated rates of seismicity compared to other parts of the plate [*Leonard*, 2008; *Leonard and Clark*, 2011].

4.3. Fragmentation of the Indo-Australian Plate

Termination of the Java trench part of the Sunda Arc subduction zone at the continental margin of western Australia is causing internal deformation of the Indo-Australian plate. Although geodetic monitoring of deformation on the Australian continent shows minimal contraction rates (best estimate range of 0.5 to 1.0 mm yr^{-1}) across the entire continent [*Tregoning*, 2003; *Leonard*, 2008], all monitoring station locations in western Australia are located inboard (e.g., at Karratha) of the reactivated faults that lie along the offshore extended margin (Figure 2, inset). Therefore, the geodetic network is not suitably designed to detect the ongoing geological deformation along the Western Australia Shear Zone. The triggered deformation within the western Australia part of the Indo-Australian plate is attributable to changes in the structural orientation,

style of deformation, and plate motion vectors along the northern plate boundary. This is analogous to the intraplate deformation occurring in the Wharton basin in the central Indian Ocean, south of the transition from the Himalayan collision to the Sagaing fault and Andaman subduction zone [*Delescluse and Chamot-Rooke*, 2007]. The intraplate deformation resulting from this plate boundary transition has caused nine earthquakes that range in magnitude from M_w 7.2 to 8.7, including the 11 April 2012 event, one of the largest shallow crustal strike slip earthquakes ever recorded [*Pollitz et al*., 2012; *Yue et al*., 2012].

The intraplate deformation in the Wharton basin is occurring in the central interior part of the Indian Ocean crust, whereas the deformation on the North West Shelf is occurring along the transition from continental to oceanic crust on the former rifted margin. The intraplate deformation along the western Australia continental margin has produced a Quaternary active strike slip fault system that may eventually evolve into a new plate boundary that decouples Indian Ocean crust from the Australian continent. Large earthquakes related to this zone of intraplate deformation include the 1943 M_L 7.3 Meeberrie and 1906 M_S 7.8 Exmouth events and faults within this zone are capable of producing future large-magnitude earthquakes. The observed geological deformation and seismic activity in the northwest Australian part of the Indo-Australia plate demonstrates that this part of the plate should not be described as a perfectly rigid block as done in several global plate motion models [*Kreemer et al*., 2003; *Delescluse and Chamot-Rooke*, 2007]. Rather, there is internal deformation along the former rifted margin caused by the transition between convergent margin types on the northern plate boundary.

5. Conclusions

We have analyzed geological, geophysical, and seismological data from a 350,000 km^2 area along the northern part of Australia's North West Shelf. These data demonstrate the presence of a system of predominantly transcurrent faults that extend along the margin of western Australia. The characteristics of this fault system are summarized below:

1. The faults coincide with northeast trending gravity anomalies that define major basin structures along the former extended margin of the Australian plate;
2. The fault system in Browse and Roebuck basins contains two primary fault zones, one along the eastern margin of the basins, and one which follows the approximate axis of the basins;
3. Focal mechanism solutions derived from earthquakes in the area between ~20°S and the northern boundary of the Indo-Australian plate are consistent with right-lateral strike slip deformation on northeast trending fault planes;
4. Faults within northern Browse basin have a dominant N70°E to N80°E fault trend but change to a N35°E to N50°E trend south of Scott Reef, representing a fundamental change in structural orientation and style;
5. The fault zones in northern Browse basin and southern Roebuck basin demonstrate a dominant down-to-the-west transcurrent sense of deformation but may locally have a down-to-the-east component;
6. Maximum rates of vertical down-to-the-west deformation range from 0.14 to 0.26 mm yr^{-1} (Table 6), consistent with geomorphic indicators of coastal subsidence;
7. Approximated maximum horizontal slip rate values across the Western Australia Shear Zone range from 1.4 to 2.6 mm yr^{-1} with average values of 0.56 to 0.65 mm yr^{-1} (Table 6);
8. Stratigraphic indicators suggest that the current period of fault reactivation coincides with the time when Australian continental crust blocked the westernmost part of the Banda arc subduction between 1 and 3 Ma;
9. Alignment of the former extended continental margin of western Australia with the transition from Java trench subduction to arc-continent collision is inferred to have triggered a new phase of fault reactivation and intraplate deformation within the Indo-Australian plate;
10. The geographic extent and characteristics of faulting indicate that the plate is not a perfectly rigid block as assumed in many plate motion models;
11. The styles of deformation along the (a) Java trench; (b) Flores-Wetar thrust, Timor trough, and Banda tectonic collision zone; and (c) the intraplate Western Australia Shear Zone are consistent with a triple junction geometry; and
12. Individual fault segments within the Western Australia Shear zone are up to 250 km in length and therefore are capable of generating earthquakes in the $7 < M < 8$ range.

Acknowledgments

We gratefully acknowledge the financial support provided by the Chevron Australia Business Unit (project PDEP AES 12-P1ABU-82). This work forms part of the activities of the Centre for Offshore Foundation Systems (COFS), currently supported as a node of the Australian Research Council Centre of Excellence for Geotechnical Engineering. We are grateful to James Dirstein and Alistair Stanley at TotalDepth, Pty for providing processing and images from the North Browse survey and to James Humphrey at Lahonton Geoscience for assistance with processing focal mechanism solutions. Seismic data are available through Geoscience Australia [*Cortese et al*., 1994].

References

Australian Geological Survey Organization North West Shelf Study Group (1994), Deep reflections on the North West Shelf: Changing perceptions of basin formation, in *The Sedimentary Basins of Western Australia*, vol. 1, pp. 63–76, Petroleum Exploration Society of Australia, Perth, Wa.

Audley-Charles, M. G. (1975), The Sumba fracture: A major discontinuity between eastern and western Indonesia, *Tectonophysics*, *26*, 213–228.

Audley-Charles, M. G. (1985), The Sumba enigma: Is Sumba a diapiric fore-arc nappe in process of formation? in *Collision Tectonics: Deformation of Collisional Lithosphere*, *Tectonophysics*, vol. 119, edited by N. L. Carter and S. Uyeda, pp. 435–449.

Audley-Charles, M. G. (2004), Ocean trench blocked and obliterated by Banda forearc collision with Australian proximal continental slope, *Tectonophysics*, *389*, 65–79, doi:10.1016/j.tecto.2004.07.048.

Audley-Charles, M. G. (2011), Tectonic post-collision processes in Timor, in *The SE Asian Gateway: History and Tectonics of the Australia–Asia Collision*, edited by R. Hall, M. A. Cottam, and M. E. J. Wilson, *Geol. Soc. London Spec. Publ.*, *355*, 235–260.

Bally, A. W. (1983), Seismic expression of structural styles, *Stud. Geol.*, *15*(3).

Berryman, K., et al. (2015), The GEM Faulted Earth subduction characterisation project, version 2.0, GEM Faulted Earth project. [Available at http://www.nexus.globalquakemodel.org/gem-faulted-earth/posts.]

Bird, P. (2003), An updated digital model of plate boundaries, *Geochem. Geophys. Geosyst.*, *4*(3), 1027, doi:10.1029/2001GC000252.

Bock, Y., L. Prawirodirdjo, J. F. Genrich, C. W. Stevens, R. McCaffrey, C. Subarya, S. S. O. Puntodewo and E. Calais (2003), Crustal motion in Indonesia from Global Positioning System measurements, *J. Geophys. Res.*, *108*(B8), 2367, doi:10.1029/2001JB000324.

Bourget, J., R. B. Ainsworth, G. Backe, and M. Keep (2012), Tectonic evolution of the "Giant" Bonaparte Continental Shelf: Impact on sediment distribution during the Pleistocene, *Aust. J. Earth Sci.*, *59*, 877–897.

Breen, N. A., E. A. Silver, and S. Roof (1989), The Wetar back-arc thrust belt, Eastern Indonesia: The effect of accretion against an irregularly shaped arc, *Tectonics*, *8*, 803–820, doi:10.1029/TC008i001p00085.

Cathro, D. L., and G. D. Karner (2006), Cretaceous-Tertiary inversion history of the Dampier Sub-basin, northwest Australia: Insights from quantitative basin modelling, *Mar. Pet. Geol.*, *23*, 503–526.

Chamot-Rooke, N., and X. L. Pichon (1999), GPS determined eastward Sundaland motion with respect to Eurasia confirmed by earthquakes slip vectors at Sunda and Philippine trenches, *Earth Planet. Sci. Lett.*, *173*, 439–455.

Clark, D., A. McPherson, and R. Van Dissen (2012), Long-term behaviour of Australian stable continental region (SCR) faults, *Tectonophysics*, *566*, 1–30.

Collins, L. B. (2002), Tertiary foundations and Quaternary evolution of coral reef systems of Australia's North West Shelf, in *The Sedimentary Basins of Western Australia*, vol. 3, edited by M. Keep and S. J. Moss, pp. 129–152, Petrol. Explor. Soc. of Australia, Perth, Wa.

Collins, L. B., and V. Testa (2010), Quaternary development of resilient reefs on the subsiding Kimberley continental margin, Northwest Australia, *Braz. J. Oceanogr.*, *58*(SPE1), 67–77.

Cortese, A., M. Tully, and A. Fleming (2014), *2014 Acreage Release Data Package*, Geoscience Australia, Canberra.

Delescluse, M., and N. Chamot-Rooke (2007), Instantaneous deformation and kinematics of the India–Australia Plate, *Geophys. J. Int.*, *168*, 818–842.

DeMets, C., R. Gordon, D. Argus, and S. Stein (1994), Effects of recent revisions to the geomagnetic reversal time scale on estimates of current plate motions, *Geophys. Res. Lett.*, *21*, 2191–2194, doi:10.1029/94GL02118.

Deplus, C., M. Diament, H. Hébert, G. Bertrand, S. Dominguez, J. Dubois, J. Malod, P. Patriat, B. Pontoise, and J.-J. Sibilla (1998), Direct evidence of active deformation in the eastern Indian oceanic plate, *Geology*, *26*(2), 131–134.

Duffy, B., M. Quigley, R. Harris, and U. Ring (2013), Arc-parallel extrusion of the Timor sector of the Banda arc-continent collision, *Tectonics*, *32*, 641–660, doi:10.1002/tect.20048.

Dziewonski, A. M., T.-A. Chou, and J. H. Woodhouse (1981), Determination of earthquake source parameters from waveform data for studies of global and regional seismicity, *J. Geophys. Res.*, *86*, 2825–2852, doi:10.1029/JB086iB04p02825.

Ekström, G., M. Nettles, and A. M. Dziewonski (2012), The global CMT project 2004–2010: Centroid-moment tensors for 13,017 earthquakes, *Phys. Earth Planet. Inter.*, *200–201*, 1–9, doi:10.1016/j.pepi.2012.04.002.

Fleury, J. M., M. Pubellier, and M. de Urreiztieta (2009), Structural expression of forearc crust uplift due to subducting asperity, *Lithos*, *113*(1), 318–330.

Fredrich, J., R. McCaffrey, and D. Denham (1988), Source parameters of seven large Australian earthquakes determined by body waveform inversion, *Geophys. J. Int.*, *95*(1), 1–13.

Gallagher, S. J., M. W. Wallace, P. W. Hoiles, and J. M. Southwood (2014), Seismic and stratigraphic evidence for reef expansion and onset of aridity on the Northwest Shelf of Australia during the Pleistocene, *Mar. Pet. Geol.*, *57*, 470–481.

Geller, R. J., and H. Kanamori (1977), Magnitudes of great shallow earthquakes from 1904 to 1952, *Bull. Seismol. Soc. Am.*, *67*, 587–598.

Genrich, J. F., Y. Bock, R. McCaffrey, E. Calais, C. W. Stevens, and C. Subarya (1996), Accretion of the southern Banda arc to the Australian plate margin determined by Global Positioning System measurements, *Tectonics*, *15*, 288–295, doi:10.1029/95TC03850.

Geoscience Australia (2009), Onshore Bouguer offshore Freeair gravity geodetic, *Geoscience Australia, Canberra*, doi:10.4225/25/5625EB0FF1471.

Hall, R. (2011), Australia–SE Asia collision: Plate tectonics and crustal flow, in *The SE Asian Gateway: History and Tectonics of the Australia–Asia Collision*, vol. 355, 73–104, edited by R. Hall, M. A. Cottam, and M. E. J. Wilson, pp. 73–104, Geol. Soc. London Spec. Publ.

Hamilton, W. (1979), Tectonic map of the Indonesian Region, *U.S. Geol. Surv. Misc. Invest. Ser.*

Harris, R., M. W. Vorkink, C. Prasetyadi, E. Zobell, N. Roosmawati, and M. Apthorpe (2009), Transition from subduction to arc-continent collision: Geologic and neotectonic evolution of Savu Island, Indonesia, *Geosphere*, *5*(3), 152–171.

Harris, R. A. (1991), Temporal distribution of strain in the active Banda orogen: A reconciliation of rival hypotheses, *J. Southeast Asian Earth Sci.*, *6*, 373–386.

Harris, R. A. (2006), Rise and fall of the Eastern Great Indonesian arc recorded by the assembly, dispersion and accretion of the Banda Terrane, Timor, *Gondwana Res.*, *10*, 207–231.

Hengesh, J. V., and B. B. Whitney (2014), Quaternary reactivation of Australia's western passive margin: Inception of a new plate boundary? in *International Union for Quaternary Research (INQUA) Focus Group on Paleoseismology and Active Tectonics, 5th International INQUA Meeting on Paleoseismology, Active Tectonics and Archeoseismology (PATA), 21–27 September 2014, Busan, Korea*, edited by C. Grutzner et al., pp. 207–210, Int. Union Quat. Res.

Hengesh, J. V., B. B. Whitney, and A. Rovere (2011), A tectonic influence on seafloor stability along Australia's North West Shelf, *Proceedings of the Twenty-first (2011) International Offshore and Polar Engineering Conference*, Maui, Hawaii, 19–24 Jun.

Jacob, K. H., and R. L. Quittmeyer (1979), The Makran region of Pakistan and Iran: Trench-arc system with active plate subduction, *Geodynam. Pakistan*, *305*, 317.

Keep M., and M. Harrowfield (2008), Elastic flexure and distributed deformation along Australia's North West Shelf: Neogene tectonics of the Bonaparte and Browse basins, in *The Nature and Origin of Compressive Margins*, vol. 306, edited by H. Johnson, et al., pp. 185–200, Geol. Soc. London Spec. Publ.

Keep, M., C. M. Powell, and P. W. Baillie (1998), Neogene deformation of the North West Shelf, Australia, in *The Sedimentary Basins of Western Australia*, vol. 2, edited by P. G. Purcell and R. R. Purcell, pp. 81–91, Petrol. Explor. Soc. of Australia, Perth, WA.

Keep, M., I. Longley, and R. Jones (2003), Sumba and its effect on Australia's north west margin, in *The Evolution and Dynamics of the Australian Plate Geol. Soc. Aust. Spec. Publ., 22*, edited by R. R. Hillis and R. D. Muller, pp. 303–312.

Keep, M., M. Harrowfield, and W. Crowe (2007), The Neogene tectonic history of the North West Shelf, Australia, *Explor. Geophys.*, *38*, 151–174.

Keep, M., J. Hengesh, and B. B. Whitney (2012), Natural seismicity and tectonic geomorphology reveal regional transpressive strain in northwestern Australia, *Aust. J. Earth Sci.*, *59*(3), 341–354.

Keep, M. A., and S. J. Moss (2000), Basement reactivation and control of Neogene structures in Outer Browse basin, North West Shelf, *Explor. Geophys.*, *31*, 424–432.

Kreemer, C., W. E. Holt, and A. J. Haines (2003), An integrated global model of present-day plate motions and plate boundary deformation, *Geophys. J. Int.*, *154*(1), 8–34.

Lajoie, K. R., D. J. Ponti, C. L. Powell II, S. A. Mathieson, and A. M. Sarna-Wojcicki (1991), Emergent marine strandlines and associated sediments, coastal California; A record of Quaternary sea-level fluctuations, vertical tectonic movements, climatic changes, and coastal processes, in *Quaternary Nonglacial Geology of the Conterminous U.S. the Geology of North America*, vol. K-2, edited by R. B. Morrison, pp. 190–203, Geol. Soc. of Am., Boulder, Colo.

Langhi, L., N. B. Ciftci, and G. D. Borel (2011), Impact of lithospheric flexure on the evolution of shallow faults in the Timor foreland system, *Mar. Geol.*, *284*, 40–54.

Leonard, M. (2008), One hundred years of earthquake recording in Australia, *Bull. Seismol. Soc. Am.*, *98*, 1458–1470.

Leonard, M., and D. Clark (2011), A record of stable continental region earthquakes from Western Australia spanning the late Pleistocene: Insights for contemporary seismicity, *Earth Planet. Sci. Lett.*, *309*(3), 207–212.

McCaffrey, R. (1988), Active tectonics of the eastern Sunda and Banda Arcs, *J. Geophys. Res.*, *93*, 15,163–15,182, doi:10.1029/JB093iB12p15163.

Nugroho, H., R. Harris, A. W. Lestariya, and B. Maruf (2009), Plate boundary reorganization in the active Banda Arc-continent collision: Insights from new GPS measurements, *Tectonophysics*, *479*(1–2), 52–65.

Pacheco, J. F., and L. R. Sykes (1992), Seismic moment catalog of large shallow earthquakes, 1900 to 1989, *Bull. Seismol. Soc. Am.*, *82*(3), 1306–1349.

Pollitz, F. F., R. S. Stein, V. Sevilgen, and R. Bürgmann (2012), The 11 April 2012 east Indian Ocean earthquake triggered large aftershocks worldwide, *Nature*, *490*(7419), 250–253.

Revets, S. A., M. Keep, and B. L. N. Kennett (2009), NW Australian intraplate seismicity and stress regime, *J. Geophys. Res.*, *114*, B10305, doi:10.1029/2008JB006152.

Rigg, J. W., and R. Hall (2011), Structural and stratigraphic evolution of the Savu Basin, Indonesia, *Geol. Soc. London Spec. Publ.*, *355*(1), 225–240.

Robb, M. S., B. Taylor, and A. M. Goodliffe (2005), Re-examination of the magnetic lineations of the Gascoyne and Cuvier Abyssal Plains, off NW Australia, *Geophys. J. Int.*, *163*, 42–55.

Rohling, E. J., K. Grant, M. Bolshaw, A. P. Roberts, M. Siddall, C. Hemleben, and M. Kucera (2009), Antarctic temperature and global sea level closely coupled over the past five glacial cycles, *Nat. Geosci.*, *2*(7), 500–504.

Roosmawati, N., and R. Harris (2009), Surface uplift history of the incipient Banda arc-continent collision: Geology and synorogenic foraminifera of Rote and Savu Islands, Indonesia, *Tectonophysics*, *479*(1), 95–110.

Saqab, M. M., and J. Bourget (2015), Structural style in a young flexure-induced oblique extensional system, north-western Bonaparte Basin, Australia, *J. Struct. Geol.*, *77*, 239–259.

Shulgin, A., H. Kopp, C. Mueller, E. Lueschen, L. Planert, M. Engels, E. R. Flueh, A. Krabbenhoeft, and Y. Djajadihardja (2009), Sunda-Banda arc transition: Incipient continent-island arc collision (northwest Australia), *Geophys. Res. Lett.*, *36*, L10304, doi:10.1029/2009GL037533.

Silver, E. A., R. Reed, R. McCaffrey, and Y. Joyodiwiryo (1983), Back arc thrusting in the eastern Sunda arc, Indonesia: A consequence of arc-continent collision, *J. Geophys. Res.*, *88*, 7429–7448, doi:10.1029/JB088iB09p07429.

Simpson, A., and M. Cooper (2008), Description, distribution and potential CO_2 storage/seal capacity of the Cenozoic sandstones and carbonates, Browse basin, Western Australia, *Geoscience Australia Record 2008/13*.

Snyder, D. B., J. Milsom, and H. Prasetyo (1996), Geophysical evidence for local indentor tectonics in the Banda Arc east of Timor, in *Tectonic Evolution of SE Asia*, edited by R. Hall, and D. J. Blundell, *Geol. Soc. London Spec. Publ.*, *106*, 61–73.

Spakman, W., and R. Hall (2010), Surface deformation and slab-mantle interaction during Banda Arc subduction rollback, *Nat. Geosci.*, *3*, 562–566.

Stewart, A. J., O. L. Raymond, J. M. Totterdell, W. Zhang, and R. Gallagher (2013), Australian Geological Provinces, 2013.01 edition, scale 1:2500000, *Geoscience Australia*, Canberra, Australia.

Storchak, D. A., D. Di Giacomo, I. Bondár, E. R. Engdahl, J. Harris, W. H. K. Lee, A. Villaseñor, and P. Bormann (2013), Public release of the ISC-GEM global instrumental earthquake catalogue (1900–2009), *Seismol. Res. Lett.*, *84*(5), 810–815, doi:10.1785/0220130034.

Struckmeyer, H. I. M., J. E. Blevin, J. Sayers, J. M. Totterdell, K. Baxter, and D. L. Cathro (1998), Structural evolution of the Browse Basin, North West Shelf: New concepts from deep-seismic data, in *The Sedimentary Basins of Western Australia*, vol. 2, edited by P. G. Purcell and R. R. Purcell, pp. 345–367, Petrol. Explor. Soc. of Australia, Perth, WA.

Tregoning, P. (2003), Is the Australian plate deforming? A space geodetic perspective, in *Evolution and Dynamics of the Australian Plate, Spec. Pap. 372*, edited by R. R. Hillis and R. D. Muller, pp. 41–48, Geol. Soc. of Am.

Waelbroeck, C., L. Labeyrie, E. Michel, J. Cl Duplessy, J. F. McManus, K. Lambeck, E. Balbon, and M. Labracherie (2002), Sea-level and deep water temperature changes derived from benthic foraminifera isotopic records, *Quat. Sci. Rev.*, *21*, 295–305.

Wallace, L. M., J. Beavan, R. McCaffrey, and D. Darby (2004), Subduction zone coupling and tectonic block rotations in the North Island, New Zealand, *J. Geophys. Res.*, *109*, B12406, doi:10.1029/2004JB003241.

Wells, D. L., and K. L. Coppersmith (1994), New empirical relationships among magnitude, rupture length, rupture width, rupture area, and surface displacement, *Bull. Seismol. Soc. Am.*, *84*(4), 974–1002.

Whitney, B. B. (2015), Neotectonic deformation in the Western Australia Shear Zone, PhD Dissertation, The University of Western Australia.

Whitney, B. B., and J. V. Hengesh (2015a), Geomorphological evidence of neotectonic deformation in the Carnarvon Basin, Western Australia, *Geomorphology*, *228*, 579–596.

Whitney, B. B., and J. V. Hengesh (2015b), Geomorphological evidence for late Quaternary tectonic deformation of the Cape Region, coastal west central Australia, *Geomorphology*, *241*, 160–174.

Whitney, B. B., J. V. Hengesh, and D. Clark (2014), The Western Australia shear zone, in *International Union for Quaternary Research (INQUA) Focus Group on Paleoseismology and Active Tectonics, 5th International INQUA Meeting on Paleoseismology, Active Tectonics and Archeoseismology (PATA), 21–27 September 2014, Busan, Korea*, edited by C. Grutzner et al., pp. 162–165, Int. Union for Quat. Res.

Whitney, B. B., D. Clark, J. V. Hengesh, and P. Bierman (2015), Paleoseismology of the Mount Narryer fault zone, Western Australia: A multistrand intraplate fault system, *Geol. Soc. Am. Bull.*, *128*, 684.

Yeates, A. N., M. T. Bradshaw, J. M. Dickins, A. T. Brakel, N. F. Exon, R. P. Langford, S. M. Mulholland, J. M. Totterdell, and M. Yeung (1987), The Westralian Superbasin, an Australian link with Tethys, in *International Symposium on Shallow Tethys 2*, edited by K. G. McKenzie, pp. 199–213.

Yue, H., T. Lay, and K. D. Koper (2012), En echelon and orthogonal fault ruptures of the 11 April 2012 great intraplate earthquakes, *Nature*, *490*(7419), 245–249.

Erratum

In the originally published version of this article, Figures 13, 16, and 17 were published with errors. These errors have since been corrected and this version may be considered the authoritative version of record.